A Nd and Sr Isotopic and Trace Element Study of a Mafic-Ultramafic Dike Swarm, Laramie Range, Wyoming: Evidence for Late Archean-Early Proterozoic Rifting of the Wyoming Craton

by

Gregory A. Snyder

T-3233

A thesis submitted to the Faculty and Board of Trustees of the Colorado School of Mines in partial fulfillment of the requirements for the degree of Master of Science in Geochemistry.

Signed: _____
Gregory Alan Snyder

Golden, Colorado

Date: 9-22, 1986

Approved: _____
E. Craig Simmons,
Thesis Advisor

_____
George H. Kennedy,
Head, Department of
Chemistry and Geochemistry

Golden, Colorado

Date: 9-22- 1986

"The kernel of indisputable information is a dot in space; interpretations grow out of the desire to make this point a line, to give it direction." -----

Barry H. Lopez, Arctic Dreams, 1986.

ABSTRACT

A major swarm of ultramafic and mafic dikes trends NE-SW and cross-cuts the entire Laramie Granite-Gneiss Terrain (an area of approximately 3000 km^2) in the central and southern Laramie Range, Wyoming. The dikes as a whole are characterized by orthopyroxene as the first pyroxene to crystallize in the sequence. It is suggested that this mineralogy may be representative of the source region which was melted to produce these liquids, and not due to contamination with continental crust. The mineralogy and bulk composition of these dikes is similar to that found in chill margins and dikes associated with Pt-rich layered mafic intrusions. Indeed, the S.E. Wyoming Province is known to be anomalously high in Pt. Therefore, the study of these dikes may yield valuable information about the formation of these deposits.

Major element, petrographic, trace element, and isotopic data suggest a division of this swarm into two major sub-types: (1) a mafic suite, with 7-12% MgO, Mg# from .52 to .77, 200 to 400 ppm Ni, subequal amounts of orthopyroxene and clinopyroxene, minor olivine, slightly LREE-enriched patterns with abundances of the REE ranging from 6x to 8x chondrites, extremely positive ϵ_{Nd} (one sample), and variable initial Sr isotopic ratios (t = 2.5

Ga), with one showing significant enrichment (0.7015 - 0.7025; 0.7034, respectively); and (2) an ultramafic suite, with 18-36% MgO, Mg# from .77 to .87, 650 to 1800 ppm Ni, large amounts of olivine and/or orthopyroxene, the lowest abundances of the REE (2x to 6x chondrites) and flat REE patterns, slightly positive ϵ_{Nd} (+2 at 2.6 Ga) and variable initial Sr isotopic ratios (0.7010 - 0.7035).

Two possible models for the evolution of these dikes are presented. The first suggests that the swarm could have been formed at 2.0 Ga by the melting of a heterogeneous mantle -- one source being chondritic, the other depleted. However, this model does not fit the Sm-Nd whole-rock isochron age of 2.5 Ga, or the Sr isotopic and trace element data. The second model, though much more complex, appears to fit the bulk of the data. In this model a depleted upper mantle is melted at 2.5 Ga to form the ultramafic suite. Underplating of a depleted lower crust by this melting event melts the crust to form the mafic suite. A model similar to that for the derivation of the mafic suite has been proposed for the formation of massif-type anorthosites.

The major and trace element chemistry and mineralogy of the swarm further suggests high degrees of melting of the depleted mantle at relatively shallow depths for the

ultramafic suite. This, coupled with other data presented herein points to a major episode of crustal attenuation and rifting in earliest Proterozoic time.

TABLE OF CONTENTS

LIST OF FIGURES

LIST OF TABLES

ACKNOWLEDGEMENTS

A great many people were involved in the production of this thesis. I would like first and foremost to thank my thesis advisor, E. Craig Simmons, for the many long hours spent discussing this and other topics and for opening my eyes to the possibilities of chemical studies of magmatic processes. Gregory S. Holden (Geology Dept., CSM) originally suggested a chemical study of the Laramie Range dikes and along with George Snyder of the USGS gave invaluable guidance in the field, and openly shared unpublished petrographic, major and trace element data. I would also like to thank the other member of my thesis committee, Donald L. Macalady, and his predecessor (before his sabbatical) Patrick MacCarthy.

Ken Ludwig and Zell Peterman of the USGS-Isotope Branch in Denver graciously offered their mass-spectrometry facilities for Nd and Sr isotopic composition and REE and Rb concentration analyses. Ken Ludwig is also thanked for his patience during the author's "first steps" into the world of mass-spectrometry, and for allowing access to his plotting programs at the USGS. Invaluable hints in separation chemistry and mass-spectrometry were generously given by Kathleen Simmons of the USGS-Isotope Branch. The Ni analyses would have been impossible without the

assistance of Thomas R. Wildeman and Sonia Helle in the Department of Chemistry and Geochemistry.

Finally, I wish to thank my wife Elizabeth, without whose love, support, patience, and caring both graduate school and this thesis would have been literally impossible.

INTRODUCTION

A major swarm of ultramafic and mafic dikes (named the Kennedy Dike Swarm in the study area; Graff, et al, 1982) occurs along the southeastern margin of the Wyoming Archean Province. The dikes are found throughout the Sierra Madre, Medicine Bow, and Laramie Ranges of southern Wyoming, but are most abundant and best preserved in the Laramie Range, where they comprise up to 20% of the terrain (Holden and Snyder, 1983). Because of the distribution of the swarm, we have concentrated our study in the Laramie Range, and specifically in the central part of that range.

Orthopyroxene was the first pyroxene to crystallize from the magmas, which can be classified compositionally as komatiitic basalts to basaltic komatiites (Jensen, 1976). Liquids such as these have also been proposed as parents to platinum(Pt)-rich layered mafic intrusions such as the Bushveld Complex, South Africa (Cawthorn and Davies, 1982; Cawthorn, et al, 1981) and the Stillwater Complex, Montana, USA (Longhi, et al, 1983; Lambert, 1982). Indeed, earlier workers recognized that part of southeastern Wyoming was a Pt-rich province (Theobald and Thompson, 1968).

The purpose of this study is to examine the significance of these dikes through petrography, and major element, trace element, and isotopic geochemistry and to further our knowledge on possible geologic processes in the formation of Pt-rich mineral deposits. Evidence collected to date suggests a major period of crustal extension in the late Archean- early Proterozoic of Wyoming. At this time, mantle upwelling and shallow melting (possibly accompanied by melting of the lower crust) occurred to produce this suite.

GENERAL GEOLOGY

Mountain ranges throughout the Wyoming Province are cored by Archean rocks. The Bighorn Mountains, Wind River Mountains, Granite Mountains, Sierra Madre Mountains, Medicine Bow Mountains, Laramie Range, Hartville Uplift, and Richeau Hills all contain Archean terrains (Heimlich and Banks, 1968; Naylor, et al, 1970, and Stuckless, et al, 1985; Peterman and Hildreth, 1978; Divis, 1976, 1977; Hills, et al, 1968; Hills and Armstrong, 1974, and Johnson and Hills, 1976, and this study; G.L. Snyder and Z.E. Peterman, personal communication and unpublished data; G.L. Snyder, personal communication; respectively). The combined surficial expression and subsurface basement make up the Wyoming Archean Craton as shown in Figure 1. The Wyoming Craton is separated from other Archean terrains by the Midcontinent Region (Figure 1, inset), although it may be a southwestern extension of the Superior Province of Canada and Minnesota (Peterman, 1979; Sims and Peterman, 1986).

The Laramie Range is underlain by a basement of layered paragneiss which may be in excess of 3.0 Ga (giga-anum) in age (Table 1). Data reported by Hills and Houston (1979) give an age of 2960 $\pm$ 220 Ma (mega-anum), and unpublished data from Z.E. Peterman (personal communication) at the USGS suggests that the age may even

Figure 1:

Simplified Precambrian geology north of the Cheyenne Belt, southeastern Wyoming, U.S.A. and location of the study area. Inset on the right shows the Archean Wyoming Province boundaries in the western U.S.A. Map is after Karlstrom and Houston, 1984.

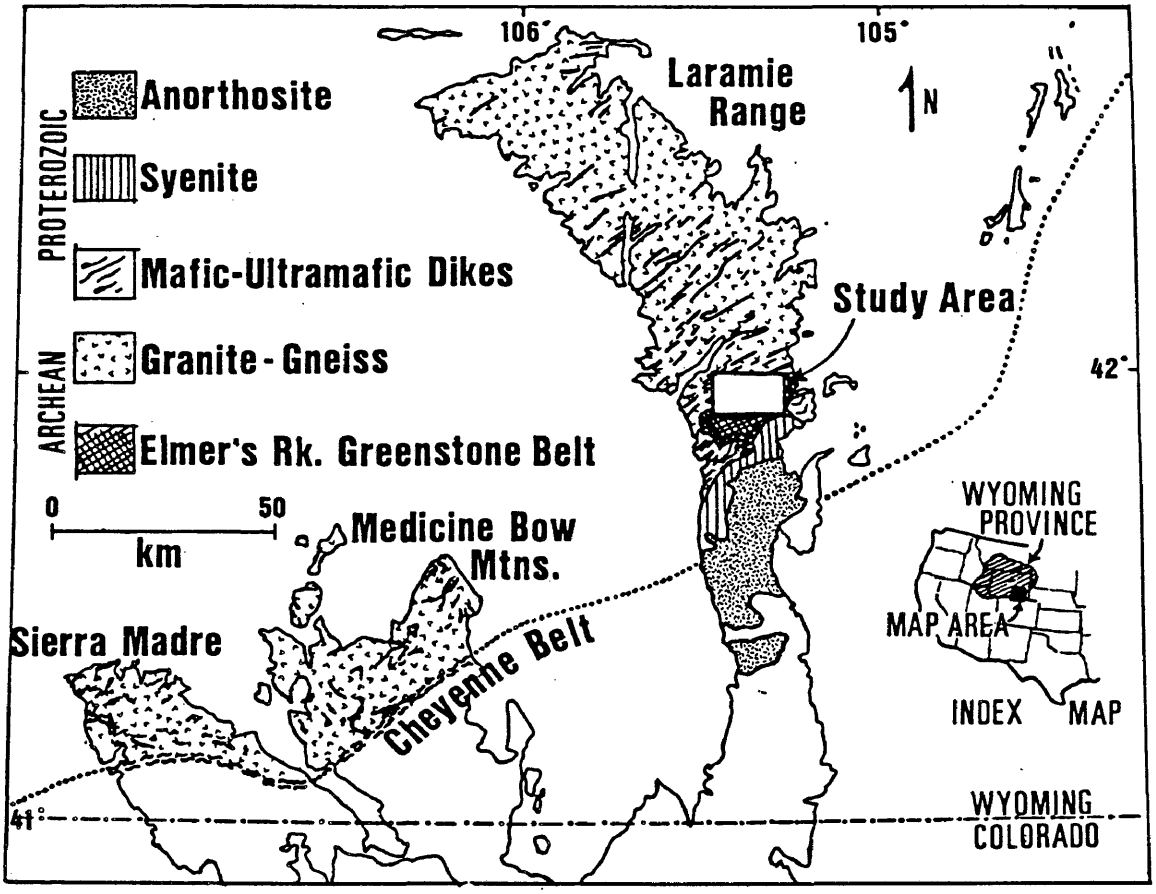

Simplified P_E Geology, S.E. Wyoming Province

Figure 1

Table 1

Chronology of Geologic Events, C. Laramie Range, Wyoming*

Event	Age
Sherman Granite	1420 ± 20 Ma (Pb-Pb, zircon)[1]
Laramie Anorthosite	1435 ± 15 Ma (U-Pb, zircon)[1]
Thermal event, continental collision?	1730 ± 60 Ma (K-Ar, hblde.)[2]
Ultramafic and mafic dikes, rifting	2530 ± 240 Ma (Sm-Nd, w-r.)[3]
Laramie Granite	2570 ± 80 Ma (Rb-Sr, w-r.)[4] 2510 ± 25 Ma (Rb-Sr, w-r.)[5]
Granite of Squaw Peak	2620 ± 30 Ma (U-Pb, zircon)[4]
Elmer's Rock Greenstone Belt	(field relations, intruded by Granite of Squaw Peak)
Laramie Gneiss Complex	2960 ± 220 Ma (Rb-Sr, w-r.)[5] 3200 Ma (Rb-Sr, w-r.)[4]

Table 1, References

*Decay constants used in calculating ages in this table and in the preceding paper are those suggested by the Subcomission on Geochronology of the IUGS (Steiger and Jager, 1977).

[1]Subbarayudu, et al, 1975

[2]Hills and Armstrong, 1974

[3]This study

[4]unpublished data, Z.E. Peterman, USGS

[5]Hills and Houston, 1979

be as old as 3200 Ma (Table 1). Field evidence points to extrusion of the Elmer's Rock Greenstone belt onto the central portion of this terrain after formation of the paragneiss. The minimum age of the greenstones is constrained by an age of 2620 $\pm$ 30 Ma from the Granite of Squaw Peak which was diapirically intruded into, and has deformed the greenstones into an arcuate pattern (G.S. Holden, personal communication, and field observation of the author). Subsequently, the voluminous Laramie Granite was intruded into the central portion of the layered paragneiss just north of the Elmer's Rock Greenstone Belt (Figure 1; Table 1).

Rb-Sr and K-Ar biotite ages decrease systematically from north to south as the southeastern edge of the Wyoming Craton is approached (Peterman and Hedge, 1978). This suggests a major thermal event at the southeastern edge of the craton, at the contact between the Wyoming Province and 1800-1600 Ma eugeosynclinal gneisses to the south in Colorado. K-Ar hornblende ages date this event at aproximately 1700 Ma (Hills and Armstrong, 1974). The contact is expressed geologically as a major shear zone, the Cheyenne Belt (also referred to in the literature as the Mullen Creek - Nash Fork Shear Zone). The systematic age decrease from north to south, and the fact that the

Cheyenne Belt is a boundary between the Archean and the Proterozoic has led some workers to postulate that this shear zone was caused by collision of the Wyoming Province with island arc successions to the south in a major accretionary event (Karlstrom and Houston, 1984). The Cheyenne Belt is not seen in the Laramie Range, but is believed to have been obliterated by the intrusion of the Laramie Anorthosite. This event was soon followed by the intrusion of the Sherman Granite in the southern Laramie Range and northern Front Range of Colorado (Table 1).

A major swarm of ultramafic--mafic dikes was intruded into the S.E. margin of the Wyoming Archean Province. These dikes (and proposed metamorphic equivalents) occur throughout the Sierra Madre and Medicine Bow Mountains, but are found in greatest abundance and are best preserved in the central Laramie Range, where they comprise up to 20% of the terrain.

These ultramafic--mafic dikes within the Laramie Range have been subdivided into four major map units by G.L. Snyder (1984): (1) peridotites -- olivine, plagioclase, enstatite, with minor clinopyroxene (cpx), biotite, magnetite, and chromite; (2) altered peridotites -- actinolite, talc, chlorite; (3) diabasic amphibolite dikes -- "granular hornblende - plagioclase - quartz -

amphibolite to cpx - hornblende - plagioclase - diabase"; and (4) plagioclase porphyry amphibolite dikes -- hornblende, plagioclase (1 to 5 cm phenocrysts), quartz amphibolites. Type (2) dikes were initially excluded from this study because they are believed to be metamorphic equivalents of type (1). Type (4) dikes were also excluded due to the intrinsic nature of this study (e.g. porphyritic samples can be exluded as possible primary liquid compositions).

This dike swarm intrudes the Archean Laramie Granite-Gneiss Terrain which has an approximate areal extent of 3000 km^2. Though ultramafic--mafic dikes occur throughout the Laramie Range (including the Preacher Creek Intrusion; Potts, et al, 1972), samples analyzed in this study come from the southern part of the terrain (Figure 2). The study area begins just north of the Elmer's Rock Greenstone Belt and is approximately 40 km north of the Cheyenne Belt -- the boundary between Proterozoic crust to the south and Archean crust to the north (Karlstrom, et al, 1984).

The dikes trend N.E.-S.W. and vary in size from several meters across to small ultramafic intrusions exceeding a kilometer in width. Most dikes are less than 200 meters in width, but can extend along strike for

Figure 2:

The study area: a portion of the Elmer's Rock Granite-greenstone terrain showing the sample locations. All sample numbers have the prefix ERGS- .


N
7-13
14
15
6
2
4
5
3
1
gneiss
greenstone
dikes
cherry ck.
peridotite
1KM
Elmer's Rock Greenstone-Gneiss Terrain: Study Area

Figure 2

several kilometers (G.L. Snyder, 1984). G.L. Snyder (1984, and personal communication) has pointed out that relative ages, as evidenced by mutually cross-cutting field relations alone, are complex.

In the field, preferential weathering of the granite--gneiss terrain has left the dikes and ultramafic intrusions exposed above the terrain as easily defineable ridges. Samples for study were collected from these ridges, which have been metamorphosed to greatly varying degrees. Metamorphism is not only variable between dikes, but also within a dike and is often associated with fractures or shear zones. Often quite pristine igneous textures within a dike will give way in a span of several centimeters to an amphibolite with small amounts of relict igneous minerals. Throughout our sampling (with the exception of ERGS-1) amphibolitized zones and dikes were avoided.

ANALYTICAL METHODS AND DATA PRESENTATION

The methods used for sample preparation and chemistry are given in detail in Appendix I. Major elements were analyzed by x-ray flourescence, Ni by atomic absorption; eight of the REE (Rare Earth Elements, or Lanthanides) and Rb and Sr by isotope dilution, and Nd was analyzed, unspiked, for isotopic composition by thermal ionization mass spectrometry (Appendix II). Typical chemical procedures found in the literature were used, with minor modifications, for the analyses of all of the afore-mentioned elements.

Nd isotopic data are discussed in terms of ϵ_{Nd} (DePaolo and Wasserburg, 1976), or deviations in parts of 10^4, at any given time (t) from a model reservoir (termed CHUR or CHondritic Uniform Reservoir):

$$\epsilon_{Nd}(t) = \left[\frac{(^{143}Nd/^{144}Nd)_{sample(t)}}{(^{143}Nd/^{144}Nd)_{chur(t)}} - 1 \right] \times 10^4$$

The reference equation for the evolution of the chondritic uniform reservoir with time is given by:

$$^{143}Nd/^{144}Nd_{BE}(t) = 0.512638 - 0.1966(e^{\lambda t} - 1)$$

where λ_{Sm} (decay constant for ^{147}Sm) = 6.54×10^{-11} $yr.^{-1}$.

The notation BE stands for the Bulk Earth model as defined by O'Nions, et al (1977). This designation is used in conjunction with the CHUR notation simply to point out that, though we are using the model reference composition defined by DePaolo and Wasserburg (1976), we are using an isotopic normalization scheme which is similar to O'Nions (i.e DePaolo and Wasserburg normalized all unspiked Nd isotopoic ratios to $^{150}Nd/^{142}Nd$ = .2096 and spiked sampled samples to $^{146}Nd/^{142}Nd$ = .636155, we normalize all ratios to $^{146}Nd/^{144}Nd$ = .7219 as per O'Nions, et al (1977), and most other labs).

The time at which a sample intersects the CHUR evolution line is designated T_{chur} and is defined by:

$$T_{chur(BE)} = 1/\lambda \times \ln \left(\frac{^{143}Nd/^{144}Nd_{sample} - {}^{143}Nd/^{144}Nd_{BE}}{^{147}Sm/^{144}Nd_{sample} - {}^{147}Sm/^{144}Nd_{BE}.} + 1 \right)$$

DePaolo (1981) also defined a depleted upper mantle reservoir which is defined by the quadratic equation:

$$\epsilon_{Nd}(t) = 0.25t^2 - 3t + 8.5.$$

Solving for T_{DM}, or the time (in Ga) at which a sample intersects the depleted mantle curve gives:

$$T_{DM} = \frac{+3 - \sqrt{0.5 + \epsilon_{Nd}(t)}}{0.5}$$

where $\epsilon_{Nd}(t) = \epsilon_{Nd}(0) - f_{Sm/Nd} * Q_{Nd} * t$. The values of $\epsilon_{Nd}(0)$ and $f_{Sm/Nd}$ are those measured at present in the rock, referenced to CHUR. The value $f_{Sm/Nd}$ is defined:

$$f_{Sm/Nd} = \frac{^{147}Sm/^{144}Nd_{sample}}{0.1966} - 1$$

and Q_{Nd} is proportional to λ_{Sm} and is equal to 25.13 Ga^{-1} (Nelson and DePaolo, 1985).

RESULTS

Locations for samples collected in this study are shown in Figure 2. Data generated from the mafic/ultramafic dikes in the central Laramie Range are presented below and in Tables 2, 3, 4, and 5. Extended petrographic descriptions are given in Appendix III.

PETROGRAPHY

The dikes vary in composition from gabbro to pyroxenite to peridotite. The thinnest dikes in the field tend to be less mafic, exhibiting a diabasic texture and containing subequal proportions of clinopyroxene (cpx) and orthopyroxene (opx), with plagioclase contents ranging from 23% to 46% by volume. The larger dikes are almost exclusively peridotitic, but may display wide variations in mineralogy and chemistry within a single intrusion (as in the Cherry Creek Peridotite Intrusion), due to mineralogic differentiation

All dikes have been through an amphibolite facies metamorphism. Although our sampling was restricted to rocks showing few effects from this event, most samples contain 5-12% fine-grained granular hornblende which rims pyroxenes, especially when in contact with plagioclase, and seems to have grown at their expense. Often associated

with the hornblende is fine-grained subhedral to euhedral garnet and very fine-grained magnetite. Magnetite is also found in association with serpentine, as an alteration product of olivine in the more ultramafic samples. Plagioclase is almost always unaltered. Samples from the large peridotitic dikes typically contain less than 5% of these metamorphic minerals.

The "diabasic" or mafic dikes generally contain little or no olivine, although in some samples clots of serpentine, magnetite, and fine-grained garnet appear to have pseudomorphously replaced preexisting olivine grains. In general, however, textural relations suggest that opx was the first mineral to crystallize. Opx is often found as subhedral to euhedral phenocrysts and often exhibits marked zoning (under plain light the rims of the opx are dark brown, in sharp contrast to the very pale brown of the cores). Some dikes exhibit a subophitic texture, with opx partially enclosing small lathes of plagioclase, but this is not the most common case. Plagioclase is typically anhedral, and interstitial in opx-rich samples. However, in less mafic samples, where cpx is dominant, plagioclase may be found as laths which are partially to completely enclosed by cpx. An contents (percent of anorthite or Ca-rich end member in the plagioclase) were determined

optically by the Michel-Levy method (Heinrich, 1965) and are quite variable, ranging from An_{35} to An_{75} even within cores. Cpx rarely forms phenocrysts and is usually found as anhedral masses interstitial to plagioclase.

Textures in the peridotitic dikes imply a crystallization sequence consistent with that found in the mafic dikes. Five of the seven peridotite samples (ERGS-7, -9, -10, -12, -13) were collected from within the same dike -- the Cherry Creek Peridotite Intrusion. Compositions within the intrusion vary widely, but the bulk of the intrusion is still peridotitic. Sample ERGS-10, though part of the intrusion and exhibiting the coarse grain size typical of the intrusion, is more similar in modal mineralogy to the mafic dikes (Table 2). Olivine and its alteration product, serpentine, often comprise one third to one half of the mode in the peridotites, and along with the other minerals, are much better preserved than in the mafic dikes. Fine- grained olivine is poikilitically enclosed by opx in most samples, and cpx is always a minor constituent. However, one sample (ERGS-12) contains large oikocrysts of cpx (augite) which enclose opx, olivine, and plagioclase. In most of these samples plagioclase is anhedral and is interstitial to all other phases. Ultramafic rocks in this study generally contain less than

Table 2

Mineralogy, Modal Abundances (vol. %)*

Mafic Suite

	ERGS-1	ERGS-3	ERGS-5	ERGS-6	ERGS-10
opx	----	26.7	24.8	20.2	18.9
cpx	13.8	15.8	15.6	23.5	20.6
plagioclase	32.3	47.5	45.7	44.1	51.8
garnet	9.1	0.5	----	----	----
opaque	3.3	----	1.3	2.9	0.4
hornblende	41.0	9.5	12.6	8.0	8.2
scapolite	----	----	----	1.3	----

Ultramafic Suite

	ERGS-4	ERGS-7	ERGS-9	ERGS-12	ERGS-13	ERGS-14	ERGS-15
opx	24.7	68.5	7.0	44.1	42.2	78.2	42.1
cpx	33.5	8.0	3.3	4.7	4.9	6.0	21.9
plagioclase	23.5	15.5	8.8	4.3	9.8	12.4	17.1
olivine	2.0	0.4	64.2	45.7	39.4	----	13.6
garnet	4.8	----	----	----	----	0.4	----
opaque	3.2	1.6	1.9	1.6	----	0.5	0.9
hornblende	8.8	3.6	----	----	0.8	1.3	4.4
scapolite	----	----	----	----	----	1.2	----
biotite	----	0.4	0.4	----	----	----	----
serpentine	----	2.0	14.4	----	2.9	----	----

*Uncertainties approximately ± 1% by volume.

20% plagioclase and up to 80% opx.

GEOCHEMISTRY

I. Major and Trace Elements

Major element compositions of the mafic-ultramafic dikes in the Laramie Range seem to support field and petrographic data which suggest a division of the samples into two sets. One set, which consists of most of the mafic dikes and sample ERGS-10, a cumulate from the Cherry Creek body, represents a "mafic suite" trend. This trend is defined by samples with <12% MgO and is further determined by a control line for the fractionation of plagioclase + opx $\pm$ olivine (Table 3; Figure 3). The second set is strictly ultramafic in nature, all samples having >18% MgO. One of the fine-grained dikes, sample ERGS-4, falls along this ultramafic or peridotite trend. Because of its occurence in the field as a thin dike with a relatively fine grain size, this sample may represent a "chilled" liquid composition. All other peridotites, which are coarse- grained and have MgO >24%, could be derived from this sample by fractionation and removal of a small amount of plagioclase and accumulation of olivine and/or orthopyroxene (Figure 3), and in subsequent discussions this sample will be included with the peridotite or

Table 3

Major Elements -- as analyzed

Mafic Suite

Sample #	ERGS-1	ERGS-3	ERGS-5	ERGS-6	ERGS-10
SiO_2	50.71	50.28	49.76	49.94	49.96
TiO_2	0.86	0.47	0.71	1.17	0.27
Al_2O_3	13.49	14.50	13.71	12.88	15.32
$Fe_2O_3^T$	11.66	8.53	10.94	13.01	6.84
MnO	0.19	0.15	0.19	0.20	0.12
MgO	8.16	11.27	9.11	7.15	11.66
CaO	11.92	12.09	12.52	11.90	13.66
Na_2O	1.79	1.44	1.63	1.44	1.17
K_2O	0.13	0.12	0.17	0.17	0.09
P_2O_5	0.08	0.05	0.07	0.08	0.04
LOI*	1.08	0.92	1.04	1.08	1.07
Total	100.07	99.82	99.84	99.01	100.20
Mg#**	0.58	0.72	0.62	0.52	0.77

Table 3 (continued)
Major Elements -- as analyzed

Ultramafic Suite

Sample #	ERGS-4	ERGS-7	ERGS-9	ERGS-12	ERGS-13	ERGS-14	ERGS-15
SiO_2	49.33	51.96	43.58	43.59	47.36	52.96	50.07
TiO_2	0.41	0.22	0.22	0.20	0.17	0.25	0.26
Al_2O_3	9.67	5.90	4.66	4.19	3.68	5.14	6.06
$Fe_2O_3^T$	10.67	9.85	10.71	11.36	10.98	10.15	11.60
MnO	0.18	0.18	0.14	0.15	0.16	0.18	0.18
MgO	18.15	24.91	34.73	35.98	33.71	25.30	25.43
CaO	9.22	6.00	4.50	3.90	3.52	5.25	5.54
Na_2O	1.04	0.23	0.11	0.29	0.11	0.21	0.34
K_2O	0.10	0.05	0.05	0.05	0.05	0.08	0.08
P_2O_5	0.05	0.02	0.02	0.02	0.02	0.02	0.02
LOI*	1.01	1.00	2.10	1.46	1.11	1.15	1.18
Total	99.82	100.31	100.81	100.18	100.87	100.69	100.76
Mg#**	0.77	0.83	0.87	0.86	0.86	0.83	0.81

^{T} Total Fe was analyzed on XRF as Fe_2O_3.

* Loss On Ignition, calculated assuming total Fe as FeO.

** Mg# = $Mg/(Mg + Fe^{2+})$.

Figure 3:

Plot of Al_2O_3 vs. MgO. This plot shows two separate trends: one contains the ultramafic suite and is defined by accumulation of the minerals olivine (OLV) and orthopyroxene (OPX) as shown by control lines (visually drawn) projecting back from the samples through these model minerals (Maaloe, 1985). The second trend contains the mafic suite and is defined by a line which bisects the model compositions of the minerals plagioclase (PLAG), clinopyroxene (CPX), and orthopyroxene (OPX) and shows fractionation of these minerals. Model mineral compositions are from Deer, Howie, and Zussman (1966).

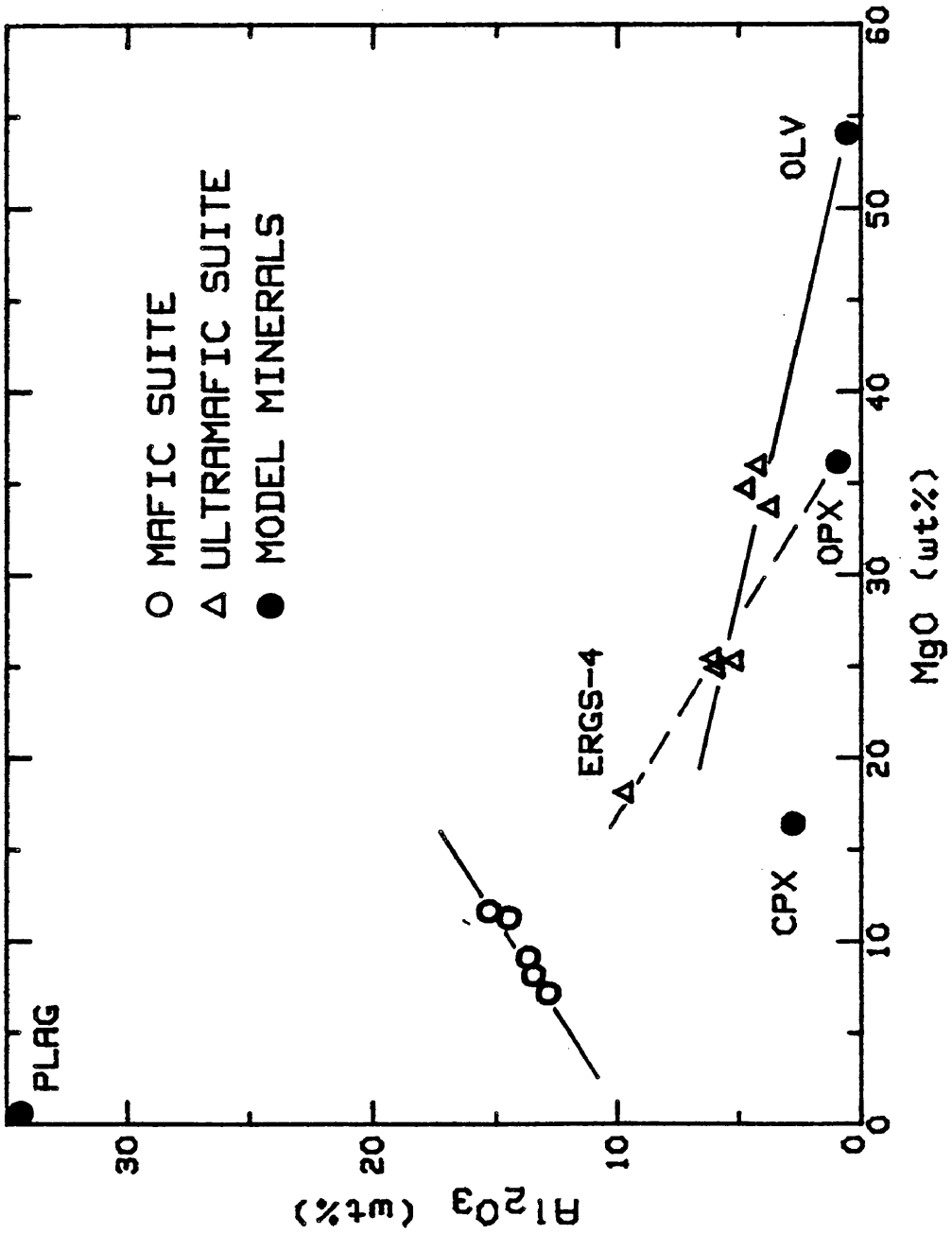
O MAFIC SUITE
Δ ULTRAMAFIC SUITE
● MODEL MINERALS
PLAG
OLV
OPX
CPX
ERGS-4
Al_2O_3 (wt%)
MgO (wt%)
0
10
20
30
40
50
60

Figure 3

ultramafic trend. The coarse-grained peridotites fall closely along an olivine control line.

Ni abundances in all samples correlate with MgO abundances and relative amounts of modal olivine (Figure 4). Ni abundances for the peridotites range from 649 to 1810 ppm, and abundances in the mafic suite vary from 182 to 376 ppm (Table 4).

The rare earth elements (REE) have been analyzed for both the peridotites and mafic suite and are given in Table 4, and plotted relative to chondrites in Figures 5 and 6. Sample ERGS-10 is not a true mafic dike (it is a plagioclase-rich cumulate -- with coarse euhedral plagioclase -- from the Cherry Creek Peridotite Body), but because it is similar to the mafic dikes in modal mineralogy and on plots of major elements and Ni, it is considered part of the mafic suite and shown with a sample of a mafic dike in Figure 5.

All of the samples have nearly chondritic proportions of the REE with only very slight light-REE enrichment. The exception to this is sample ERGS-10 which shows a slight increase in Ce/Sm compared to all other samples. Abundances of the REE correlate roughly with abundances of MgO. The samples vary in abundances from 2x to 8x chondrites and all show significant positive Eu anomalies.

Figure 4:

(a) Plot of MgO vs. Ni showing a positive linear correlation.

(b) Plot of modal olivine (vol%) vs. Ni which again shows a positive correlation.

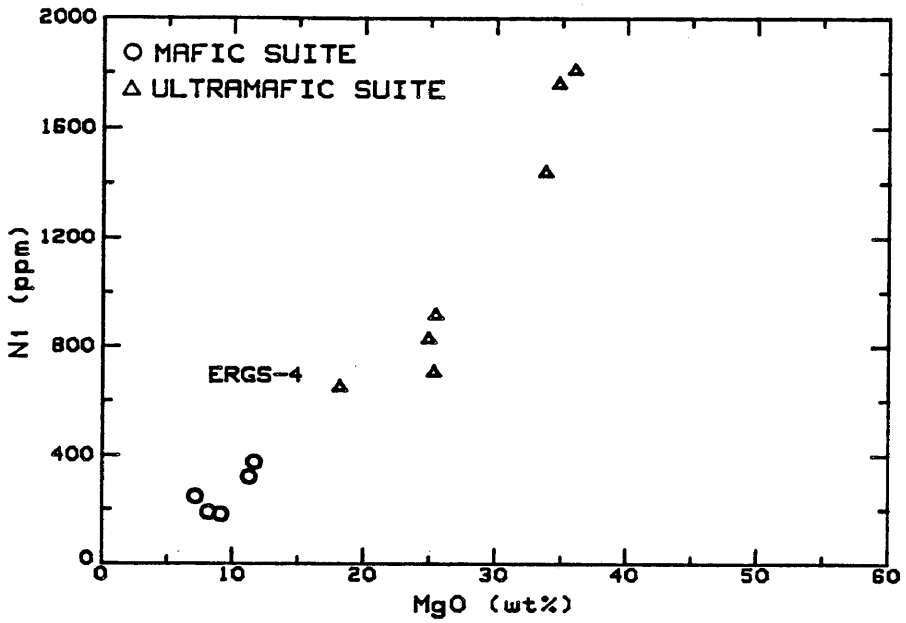
O MAFIC SUITE
Δ ULTRAMAFIC SUITE
ERGS-4
Ni (ppm)
MgO (wt%)
0
400
800
1200
1600
2000
0
10
20
30
40
50
60

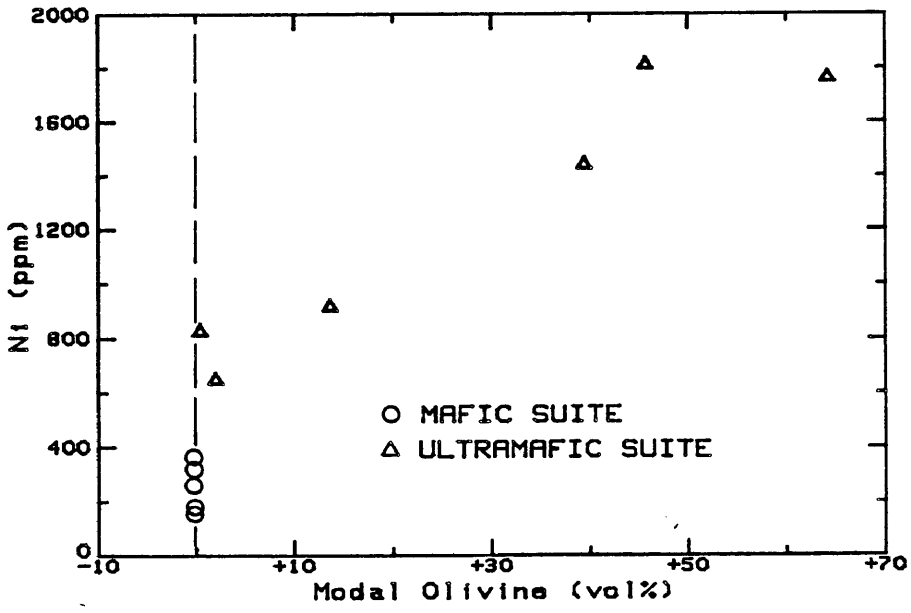
O MAFIC SUITE
Δ ULTRAMAFIC SUITE
Ni (ppm)
Modal Olivine (vol%)
0
400
800
1200
1600
2000
-10
+10
+30
+50
+70

Figure 4

Table 4
Trace Elements (ppm)

Mafic Suite

	ERGS-1	ERGS-3	ERGS-5	ERGS-6	ERGS-10
Ce[1]	----	6.38	----	----	4.57
Nd	----	4.30	----	----	2.47
Sm	----	1.27	----	----	0.679
Eu	----	0.567	----	----	0.277
Gd	----	----	----	----	0.916
Dy	----	1.87	----	----	----
Er	----	1.09	----	----	0.652
Yb	----	1.04	----	----	0.639
Ce/Sm	----	5.01	----	----	6.73
Rb[2]	----	2.870	3.929	3.112	1.958
Sr	----	103.9	90.97	134.6	80.94
Ni[3]	190	321	182	249	376

Table 4 (continued)
Trace Elements (ppm)

Ultramafic Suite

	ERGS-4	ERGS-7	ERGS-9	ERGS-12	ERGS-13	ERGS-14	ERGS-15
Ce	4.60	2.10	2.39	----	1.64	2.60	----
Nd	3.06	1.44	1.67	1.51	1.16	1.69	1.87
Sm	0.921	0.450	0.508	0.466	0.336	0.500	0.553
Eu	0.361	0.175	0.195	0.175	0.127	0.188	0.228
Gd	----	----	0.682	----	----	----	----
Dy	----	0.760	0.801	----	0.508	0.786	----
Er	0.853	0.501	0.498	----	0.327	0.506	----
Yb	0.811	0.522	0.498	----	0.341	0.523	----
Ce/Sm	4.99	4.67	4.70	----	4.89	5.20	----
Rb	2.458	1.203	0.7206	0.6781	1.083	1.668	1.858
Sr	68.82	29.91	26.26	23.78	19.13	35.19	39.58
Ni	649	827	1760	1810	1440	704	916

---

[1] Uncertainties of REE generally <0.2%.

[2] Uncertainties of Rb and Sr generally <0.5%.

[3] Uncertainties of Ni <5%.

Figure 5:

Rare earth element (REE) abundances, normalized to chondritic meteorites, of samples of the mafic suite.

Figure 6:

REE abundances, normalized to chondritic meteorites, of samples of the ultramafic or peridotite suite. Symbols are as follows: ●, ERGS-4; ▽, ERGS-15; ○, ERGS-14; ⬢, ERGS-9; □, ERGS-12; ■, ERGS-7; ▼, ERGS-13.

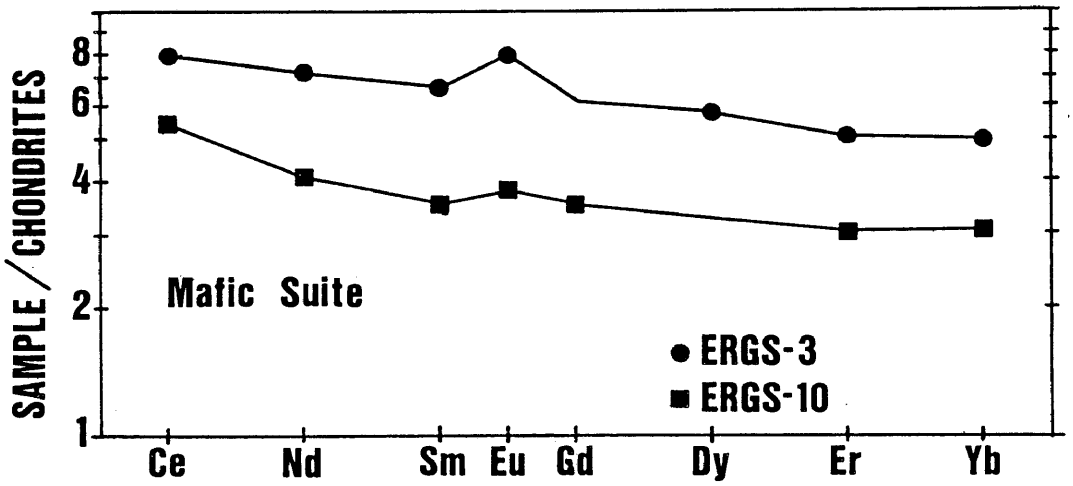

Figure 5

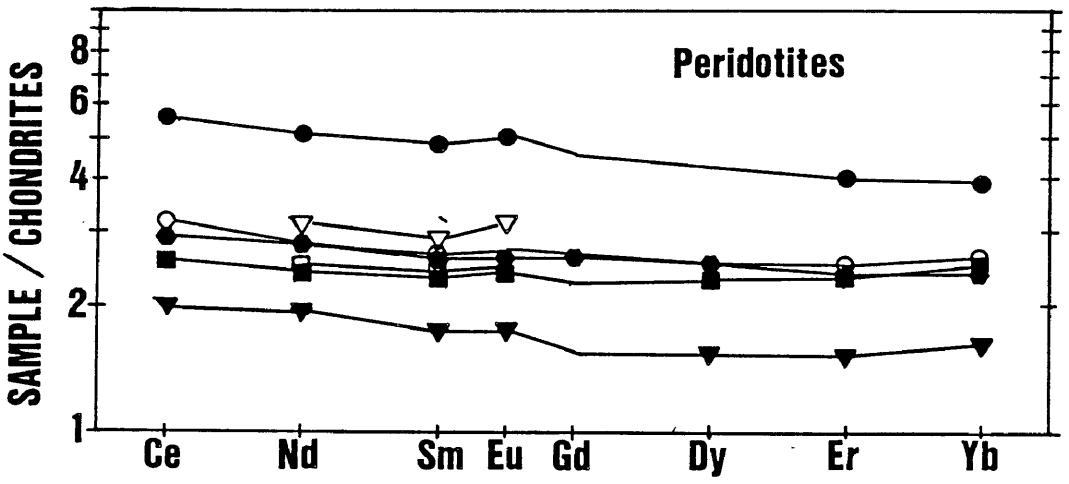

Figure 6

REE analyses of the peridotites are generally quite consistent with previous data. Sample ERGS-4 has the highest abundance of the REE and samples of peridotitic cumulates have progressively lower abundances as accumulation of minerals with low REE content progresses. REE abundances do not decrease with increasing modal% olivine and opx in the cumulate peridotites (Figure 6), but instead are determined by the amount of the relatively REE-rich phase clinopyroxene (cpx). Petrographic observations discussed earlier point to cpx as one of the final phases to crystallize in the cumulate peridotites, and it may represent, along with plagioclase, the final "trapped" liquid component. Therefore as "trapped liquid" decreases, so do abundances of the REE.

Two samples of the mafic suite are plotted on Figure 5. Sample ERGS-10 has an slightly higher Ce/Sm ratio compared to all other samples analyzed. ERGS-3 has the highest abundances of the REE analyzed and fits well with the less primitive petrographic and major element data of the mafic suite.

II. Nd AND Sr ISOTOPES

Four samples of peridotites and one sample from the mafic suite (ERGS-10) were analyzed for their Nd isotopic

Figure 7:

Sm-Nd whole-rock isochron plot: $^{147}Sm/^{144}Nd$ vs. $^{143}Nd/^{144}Nd$. (a) Enlargement of a section of figure 7(b) showing the scatter about the 2530 $\pm$ 246 Ma (Ma = mega-annum or million years) isochron for the four peridotite samples. (b) Plot showing the y-intercept of the isochron, and thus the initial ratio of 0.5094 $\pm$ 0.0003, or ϵ_{Nd} = +1.8.

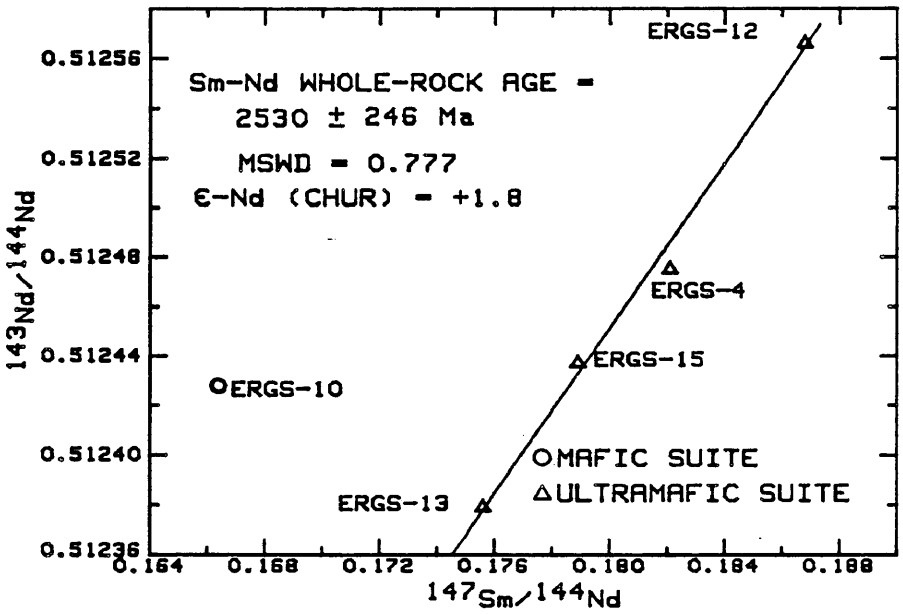
Sm-Nd WHOLE-ROCK AGE =
2530 ± 246 Ma
MSWD = 0.777
ε-Nd (CHUR) = +1.8
ERGS-12
ERGS-4
ERGS-15
ERGS-10
ERGS-13
OMAFIC SUITE
ΔULTRAMAFIC SUITE
0.51256
0.51252
0.51248
0.51244
0.51240
0.51236
0.164
0.168
0.172
0.176
0.180
0.184
0.188
143Nd/144Nd
147Sm/144Nd

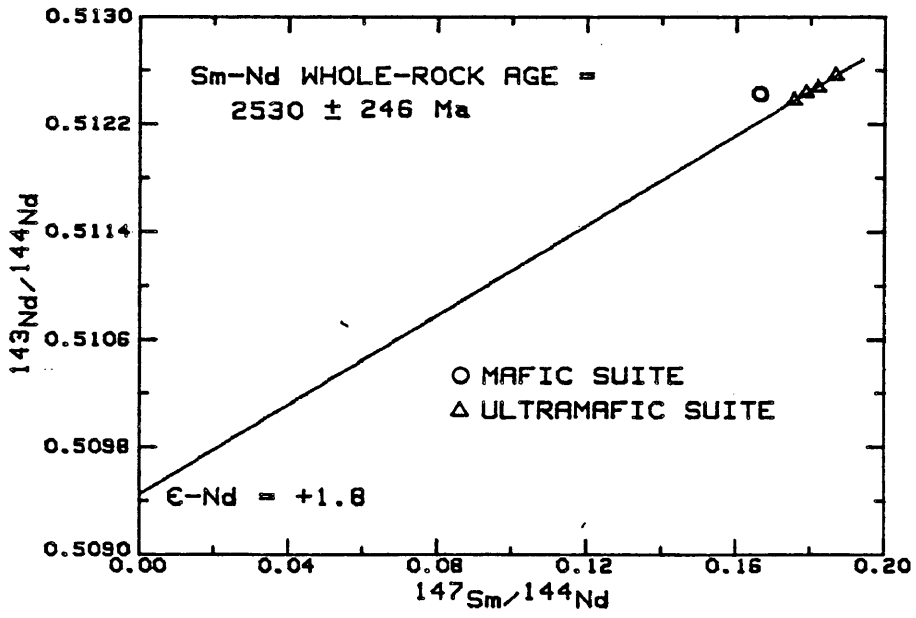
Sm-Nd WHOLE-ROCK AGE =
2530 ± 246 Ma
O MAFIC SUITE
Δ ULTRAMAFIC SUITE
ε-Nd = +1.8
0.5130
0.5122
0.5114
0.5106
0.5098
0.5090
0.00
0.04
0.08
0.12
0.16
0.20
143Nd/144Nd
147Sm/144Nd

Figure 7

Table 5

Isotopic Data

Sample #	$^{87}Rb/^{86}Sr$*	$^{87}Sr/^{86}Sr$	2-sigma	$^{147}Sm/^{144}Nd$**	$^{143}Nd/^{144}Nd$	2-sigma	T-CHUR
ERGS-3	0.07989	0.705056	2.4×10^{-5}				
	0.08211	0.705021	6.7×10^{-5}				
ERGS-4	0.1033	0.705211	2.8×10^{-5}	0.1821	0.512475	1.9×10^{-5}	1.72 Ga
ERGS-5	0.1249	0.706009	3.0×10^{-5}				
	0.1243	0.705845	8.7×10^{-5}				
ERGS-6	0.06687	0.703636	2.2×10^{-5}				
ERGS-7	0.1164	0.705361	3.9×10^{-5}	0.1887			
ERGS-9	0.07938	0.704051	3.2×10^{-5}	0.1837			
ERGS-10	0.06997	0.705667	2.3×10^{-5}	0.1664	0.512428	4.3×10^{-5}	1.07 Ga
	0.06974	0.705515	3.4×10^{-5}	0.1708[D]	0.512487[D]	2.3×10^{-5}	0.90 Ga
ERGS-12	0.08249	0.704769	2.4×10^{-5}	0.1868	0.512566	1.3×10^{-5}	1.14 Ga
ERGS-13	0.1637	0.706781	5.2×10^{-5}	0.1756	0.512379	1.7×10^{-5}	1.88 Ga
ERGS-14	0.1372	0.70839	3.6×10^{-5}				
ERGS-15	0.1358	0.706146	5.7×10^{-5}	0.1789	0.512437	1.8×10^{-5}	1.73 Ga

* 2-sigma error is $\pm$ 1 %.

** 2-sigma error is $\pm$ 0.5%.

[D] Duplicate analysis performed by Dan Unruh, USGS - Isotope Branch, Denver.

composition and are plotted on Figure 7 (data in Table 5). The four peridotites give a linear array with an age of 2530 ± 246 Ma and an initial ratio of 0.5094 ± .0003 (ϵ_{Nd} = +1.8). The one sample of the mafic suite analyzed to date, ERGS-10, lies well off of this line and suggests a source with a much higher $^{143}Nd/^{144}Nd$ ratio than the peridotites. The age for this sample is assumed to be similar to that for the peridotites, as it is a plagioclase-rich cumulate from the same body which ERGS-12 and ERGS-13 were sampled (the Cherry Creek Peridotite).

Rb-Sr isotopic data for the peridotites and the mafic suite are shown in Table 5 and Figure 8. Together, the data do not form a linear array, but instead show a great amount of scatter. One sample from the mafic suite, ERGS-10, has unsupported radiogenic Sr (e.g. this sample could not have generated the amount of radiogenic Sr found in the rock through simple decay of the amount of Rb now found in the rock; i.e. projected back in time this sample would never intersect the mantle evolution line -- an impossibility for a simple one-stage process). This sample is unlike all other samples from the mafic suite in that it is a cumulate from the Cherry Creek Peridotite body.

By arbitrarily picking points one can come up with "isochrons" of varying ages, but there seems to be no

Figure 8:

Rb-Sr diagram: plot of $^{87}Rb/^{86}Sr$ vs. $^{87}Sr/^{86}Sr$ for 11 whole-rock samples. Also plotted are two reference isochrons. The lower line corresponds to an age of 2264 $\pm$ 274 Ma (4 points regressed) and the upper line corresponds to an age of 2796 $\pm$ 43 Ma (2 points regressed). The lines were plotted using a least squares approximation method (Ludwig, 1985).

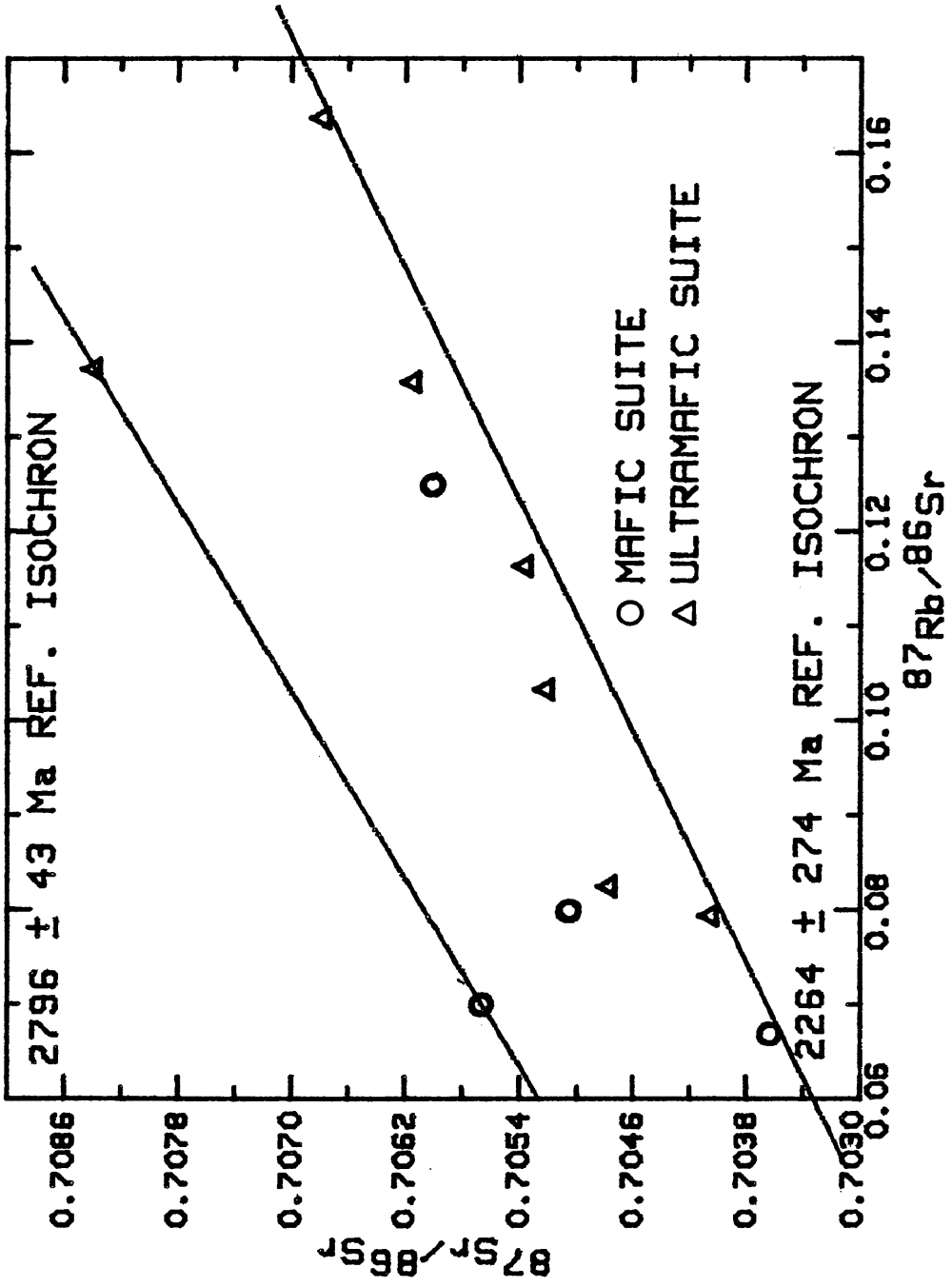
2796 ± 43 Ma REF. ISOCHRON
2264 ± 274 Ma REF. ISOCHRON
O MAFIC SUITE
Δ ULTRAMAFIC SUITE
$^{87}Sr/^{86}Sr$
$^{87}Rb/^{86}Sr$
0.7086
0.7078
0.7070
0.7062
0.7054
0.7046
0.7038
0.7030
0.06
0.08
0.10
0.12
0.14
0.16

Figure 8

logical way to discern which, if any, is most appropriate. We have tried to delineate, on the basis of mineralogical or elemental differences, different sets (such as mafic suite and ultramafic suite), but the arrays defined by these sets still scatter widely. Instead we have drawn two lines which enclose all data points. One line bounds the data at the minimum values of $^{87}Sr/^{86}Sr$ and actually fits 5 of the points quite well. This line gives an age of 2264 $\pm$ 274 Ma. An upper line was drawn through the two samples with the highest $^{87}Sr/^{86}Sr$ and gives an age of 2796 $\pm$ 43 Ma. A regression of 8 of the 11 samples which are most concordant and lie at lower $^{87}Sr/^{86}Sr$ gives an age of 2219 $\pm$ 511 and nearly spans the total range defined by the the two bounds shown in Figure 8.

DISCUSSION

Because of the nature and consistent structural trend of the ultramafic dikes and intrusions in the central Laramie Range, previous workers speculated that these intrusives were products of a major rifting episode (see references in Karlstrom and Houston, 1984). It is our belief that mineralogic, major element and isotopic data presented in this paper further support this contention.

Petrographic studies suggest that this suite may be subdivided along lines defined by the macroscopic field work (Snyder, G.L., 1984), into two sets described previously (peridotites, or ultramafic dikes, and mafic dikes). Assuming a genetic relationship between the two sets, a simplified sequence of crystallization may also be determined:

(1) olivine --> (2) opx --> (3) opx + plag -->

(4) cpx + plag + opx.

Textural observations (relatively large grain sizes and euhedral to subhedral habits of olivines and pyroxenes), along with field observations of layering, suggest that the ultramafic dikes are generally cumulates. The mafic "diabasic" dikes, due to their thinner widths in the field and much finer grain size, on the other hand would appear to represent near liquid compositions.

All of the ultramafic and mafic samples from the Laramie Range are distinguished by having orthopyroxene (opx) as the first pyroxene to appear on the solidus. This is important in light of recent work (Campbell, 1985) which suggests that primitive mantle-derived magmas would naturally have clinopyroxene (cpx) as the first crystallizing pyroxene. Campbell proposed that magmas with opx as the first crystallizing pyroxene are found most commonly in continental regions and have assimilated significant amounts of crust to arrive at this point.

However, we suggest the possibility that the opx-rich magmas in the Laramie Range reflect the mantle composition and may not simply be due to contamination. Recent work has shown that the lower crust can be quite variable in composition (AGU Spring Meeting, 1984, "Lower Continental Crust"). This makes it extremely difficult to ascertain the importance and degree of contamination due to the lower crust. In order to estimate this effect, however, we can define two limiting cases. If the lower crust beneath Wyoming during the late Archean- early Proterozoic was mafic or in fact ultramafic, then a significant percentage of assimilation of this material would be possible. In fact it is possible that the melts were completely generated from a lower crust that had the composition of,

say, a mafic layered intrusion.

In the second limiting case we can assume that the lower crust is quite felsic and has a composition analogous to intermediate values estimated in the literature (Weaver and Tarney, 1984). All samples analyzed in this study have less than 0.2% K_2O, and the peridotites (ultramafic suite) contain <0.1% K_2O. Sample ERGS-4, the suggested liquid composition for the peridotites, has 0.1% K_2O. Assuming ERGS-4 contained 0% K_2O initially, and that the Archean crust had a value of 1.0 % K_2O (intermediate literature value; typical lower crustal value of 1.0%, Weaver and Tarney, 1984), simple bulk-mixing calculations limit the amount of contamination to ERGS-4 to a maximum of 10%. However, K may act as an incompatible element during melting processes (Hughes, 1982; Watson and Jurewicz, 1984; i.e. fractionated heavily into the initial melt phase). This would further reduce the amount of possible contamination and render this untenable as a major process.

Due to the overall low values for K_2O in all samples and the fact that none show anomalously high K_2O abundances, contamination, if it did occur, must have occured early in a subcrustal magma chamber before intrusion. This would have homogenized all samples and would still allow smooth fractionation trends to be shown

on all major element plots. Contamination at the level of emplacement is not seen; in fact the opposite is found in chill margins in some dikes which have compositions (low K_2O% and high MgO%) similar to that of ERGS-4 -- a sample from the center of an ultramafic dike, and a suggested liquid composition (Snyder, G.L., personal communication, unpublished data).

The chemistry of the peridotites (ultramafic suite) suggest that they are mantle-derived. Mg#'s vary from .77 to .87, well within the possible range of values for magma in equilibrium with mantle olivine of Fo_{89} (i.e., Mg# of .72). On a plot of TiO_2 vs. Al_2O_3 (Figure 9) the peridotites lie near, but just below a line of chondritic composition, and the mafic suite forms a trend with a negative slope which is nearly perpendicular to any mantle trend (Sun, 1985). Ohtani (1984) has suggested that samples which plot along the ultramafic trend in figure 9 are derived at relatively shallow depths (<200 km) and have <u>not</u> fractionated and removed garnet at depth (therefore no depletion of Al).

Further support for a mantle derivation for the peridotites is also seen in Figure 10. On this plot, MgO and FeO have been recalculated to cation mole%, with total Fe as FeO as a limiting case (Langmuir and Hanson, 1978).

Figure 9:

Plot of Al_2O_3 vs. TiO_2. Dashed line has a slope of 10.2 and corresponds to typical Al-undepleted mantle (Sun, 1984). Dash-dot line corresponds to Al-depleted mantle source, such as that determined for Barberton komatiites (from Sun, 1984), and has a slope of 20.4.

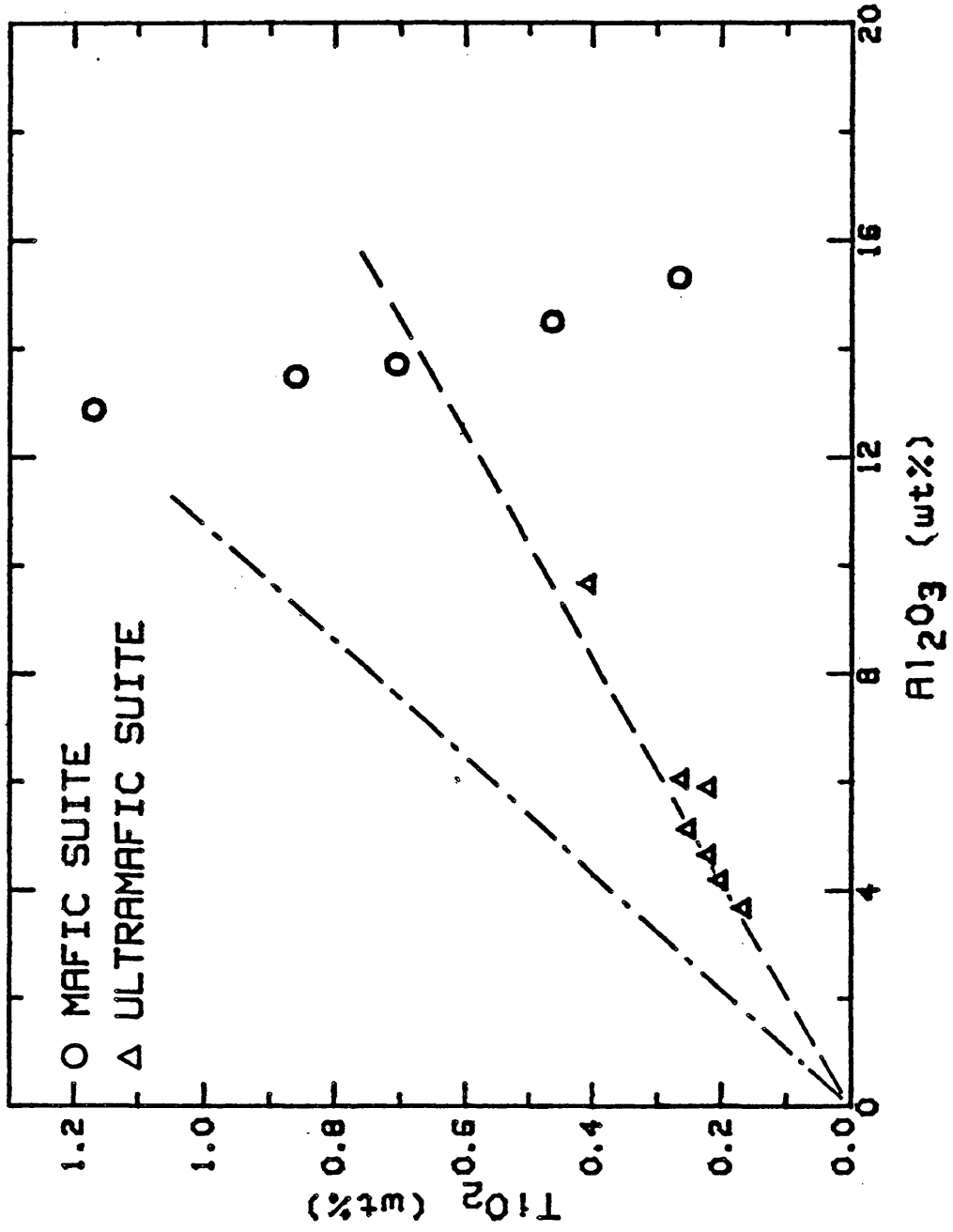
O MAFIC SUITE
Δ ULTRAMAFIC SUITE
TiO2 (wt%)
Al2O3 (wt%)
0.0
0.2
0.4
0.6
0.8
1.0
1.2
0
4
8
12
16
20

Figure 9

Figure 10:

Plot of Mg cation mole % vs. Fe cation mole % superimposed upon the melt and residue fields from melting of the mantle having a pyrolite composition, at 1 bar pressure (Langmuir and Hanson, 1978). Nearly horizontal lines are isotherms, and lines of positive slope with slight curvature are of constant percentages of melting. Curved, nearly vertical lines are olivine fractionation paths with tick marks shown for every 5% fractionation of the remaining liquid.

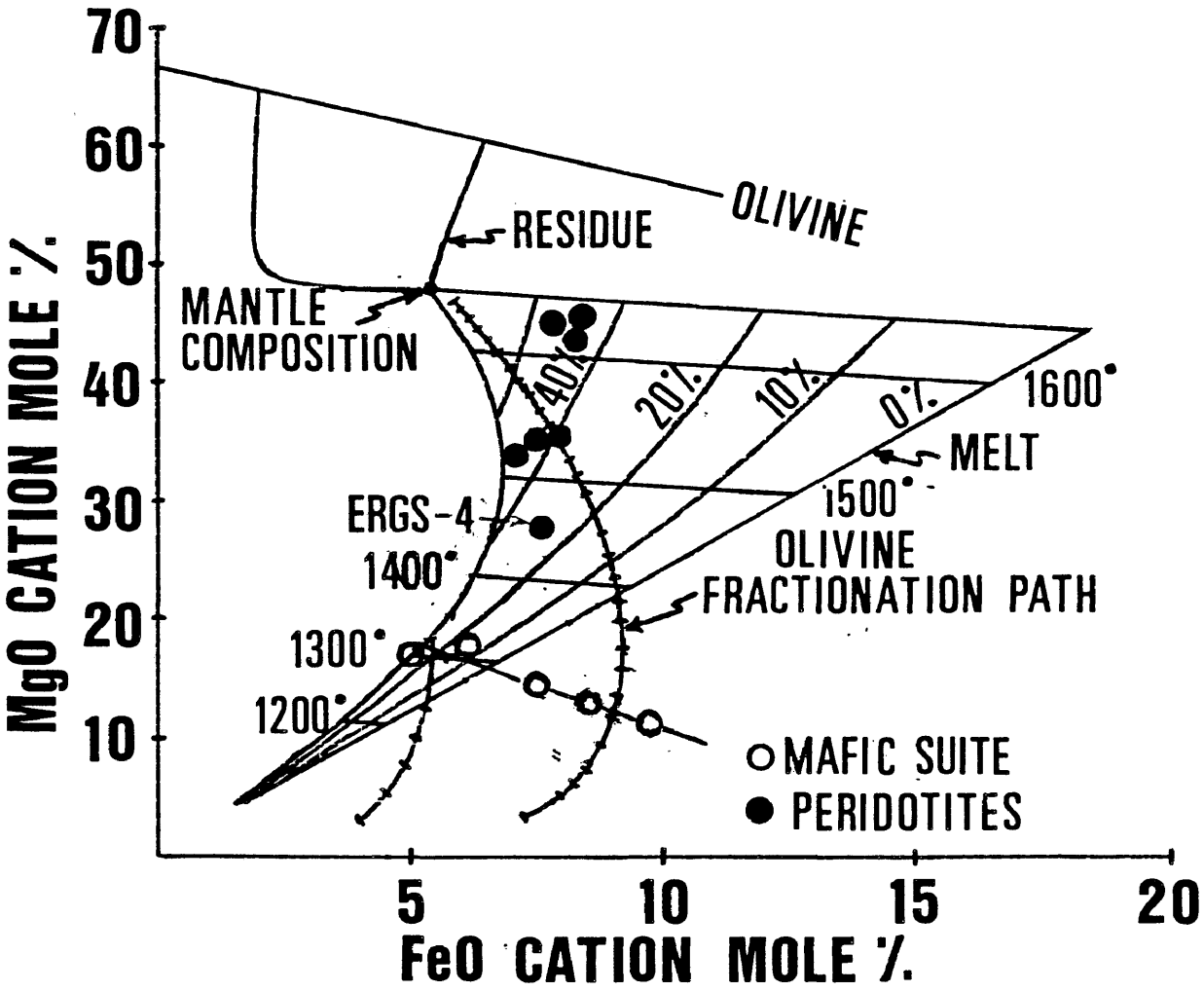
70
60
50
40
30
20
10
MgO CATION MOLE %
RESIDUE
OLIVINE
MANTLE
COMPOSITION
40%
20%
10%
0%
1600°
MELT
1500°
ERGS-4
1400°
OLIVINE
FRACTIONATION PATH
1300°
1200°
MAFIC SUITE
PERIDOTITES
5
10
15
20
FeO CATION MOLE %

Figure 10

The samples are again divided into two groups. The peridotites plot totally within the field of permissable mantle melts, though we know from mineralogy and major elements that they have accumulated a significant amount of olivine and/or orthopyroxene. ERGS-4, the suggested parental liquid to the peridotites, indicates 30% melting of a mantle of pyrolite composition at 1450°C.

The mafic suite plots along a linear nearly isothermal trend at a lower temperature, 1300°C, and suggests lower percentages of melting (the sample which gives the highest % melting for this suite is itself a cumulate, ERGS-10, and cannot be a liquid). This trend for the mafic suite could be explained by mantle melting and subsequent fractionation and removal of plagioclase and an Fe-rich phase (possibly clinopyroxene and/or chromite) to progressively deplete the magma in Fe and enrich it in Mg. The peridotites, on the other hand, show mantle derivation coupled with <u>accumulation</u> of olivine and orthopyroxene to give a nearly vertical trend.

Sample ERGS-4, a finer-grained ultramafic dike (>18% MgO, 649 ppm Ni) and the proposed parental liquid to the peridotites, is typical of all magmas and has opx as the first pyroxene to crystallize. It also contains minor amounts of modal olivine (<5%). Jaques and Green (1980)

have shown that samples of this composition, which are silica-rich, contain only minor olivine, and have opx as the initial solidus pyroxene, represent relatively high percentage mantle melts at shallow depths (Figure 11). Note that the degree of melting indicated by this diagram (30%) is similar to that determined using the MgO-FeO diagram and calculations of Langmuir and Hanson (1978). Further, the proposal of melting at a shallow depth is consistent with the Al-undepleted nature of the peridotites and experimental work of Ohtani (1984, mentioned earlier).

During widespread rifting the crust is attenuated and mantle upwelling occurs, allowing melting to occur at shallower depths. The interpretation of the peridotites as fractionates from a magma (similar to ERGS-4), which was derived at shallow depths (20-30 km) by high degrees of melting, of the upper mantle supports a rifting regime for these samples.

The wide range in Ni compositions shown by the peridotites is in good agreement with field3observations and data that these samples are formed by accumulation of olivine and are not tectonically emplaced residues of mantle melting processes (figure 8 from Frey, et al, 1985). The mafic suite on the other hand would seem to show fractionation and removal of olivine, if they are

Figure 11:

Experimental melting plot of pyrolite showing temperature vs. pressure and fields for pertinent rock compositions (Jaques and Green, 1980). Dashed lines labeled "cpx out" and "opx out" are the limits at which clinopyroxene and orthopyroxene, respectively, cease to be a major phase in the residuum. Dotted lines labeled "20%", "30%", and "50%" are the extents of melting. Parabolic curves labeled "0%", "15%", and "20%" are the relative volumetric amounts of olivine found in the crystallized products.

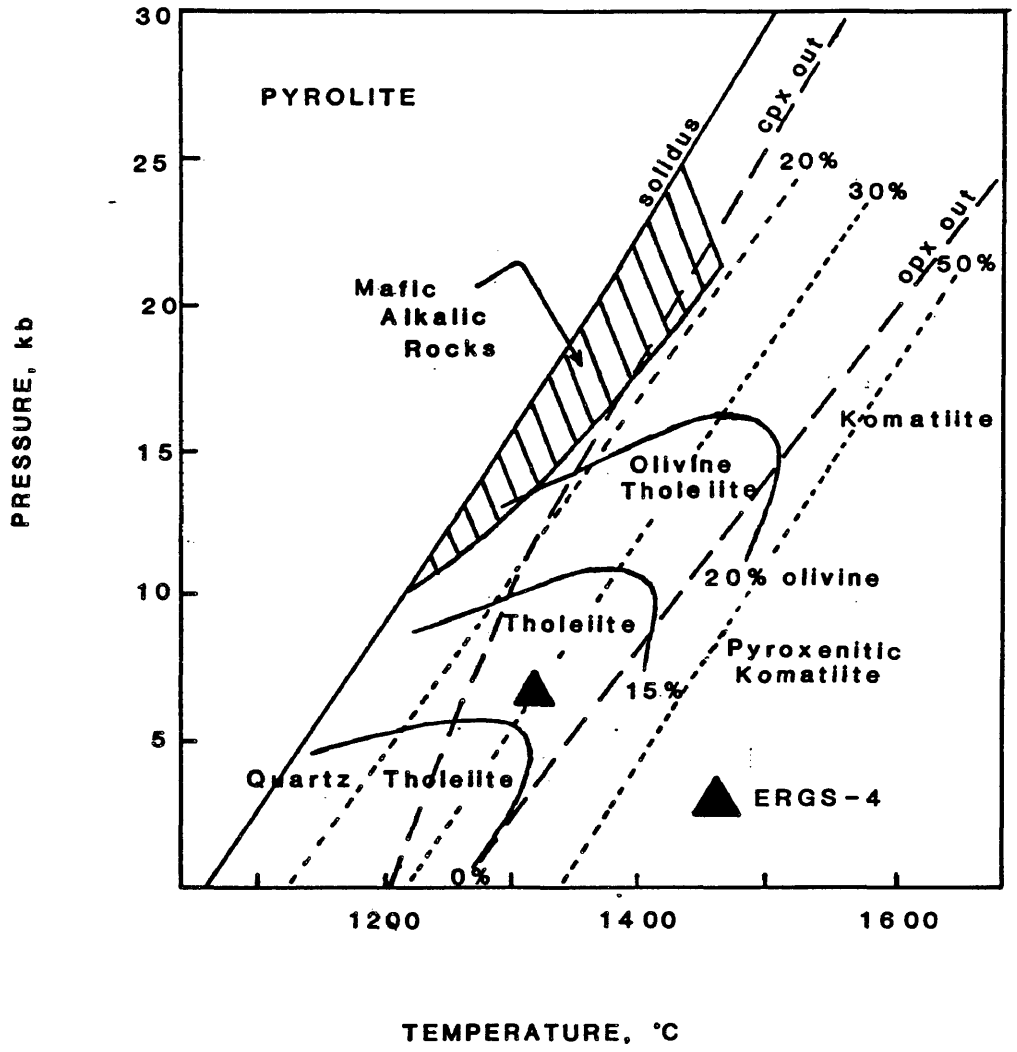
PYROLITE
solidus
cpx out
20%
30%
opx out
50%
Mafic
Alkalic
Rocks
Komatiite
Olivine
Tholeiite
20% olivine
Tholeiite
Pyroxenitic
Komatiite
15%
Quartz Tholeiite
ERGS-4
0%
30
25
20
15
10
5
1200
1400
1600
PRESSURE, kb
TEMPERATURE, °C

Figure 11

related to the peridotites at all.

Huppert and Sparks (1985) have shown experimentally that, assuming emplacement mechanisms are the same, magmas with higher emplacement temperatures will necessarily melt more country rock and therefore be contaminated to greater degrees than magmas with lower emplacement temperatures. Thus, as contamination proceeds in an ultramafic magma the temperature will fall and lower percentages of country rock will be melted (assuming the contaminating country rock is relatively homogeneous). Translated into graphic form on a diagram of Ni (a highly compatible element) vs. K_2O (oxide of the incompatible element K), this process of decreasing contamination with time will give a trend with a positive slope (Figure 12).

As shown on Figure 13, ultramafic-mafic samples from the Laramie Range give a trend with a negative slope on a Ni vs. K_2O diagram. The negative slope is most pronounced for samples from the ultramafic suite. This would then suggest a relatively uncontaminated nature to all samples, especially those of the ultramafic suite.

The cumulate peridotites (ultramafic suite) do not show a consistent decrease in REE abundances with increasing modal% olivine and opx (Figure 5), but instead seem to be coupled with the relatively REE-rich phase

Figure 12:

Plot of Ni vs. K_2O. "Hypothetical example of trends produced by fractional crystallization and contamination" (after Huppert and Sparks, 1985). The more ultramafic in character a sample is the greater the percent of contamination -- thus giving a trend with a positive slope.

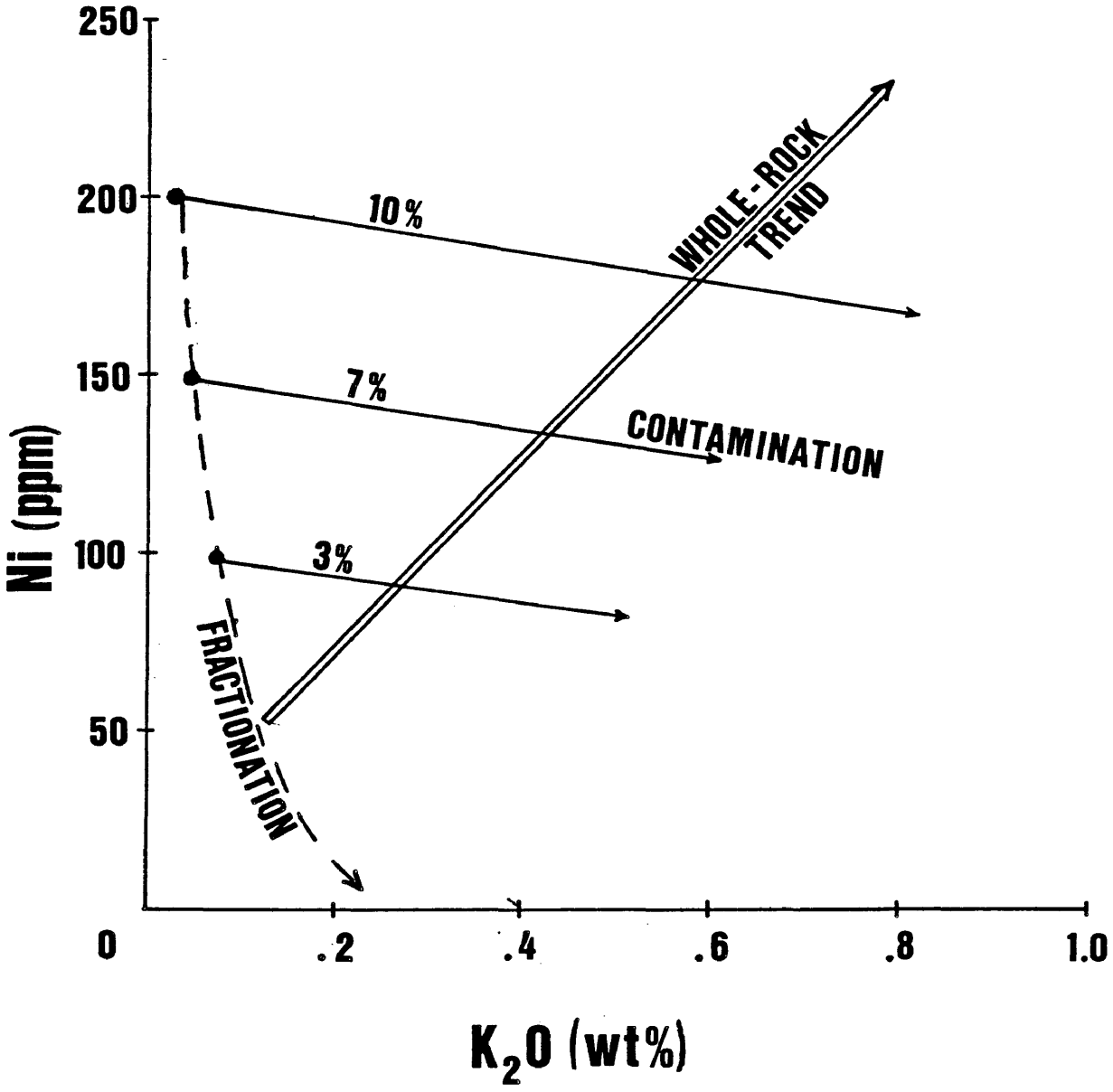
250
200
150
100
50
0
.2
.4
.6
.8
1.0
Ni (ppm)
K_2O (wt%)
10%
7%
3%
CONTAMINATION
WHOLE-ROCK TREND
FRACTIONATION

Figure 12

Figure 13:

Plot of K_2O vs. Ni showing possibly two separate trends or one continuous trend, both with negative slopes. The solid curve is drawn through the ultramafic suite and the dashed line is drawn through the mafic suite.

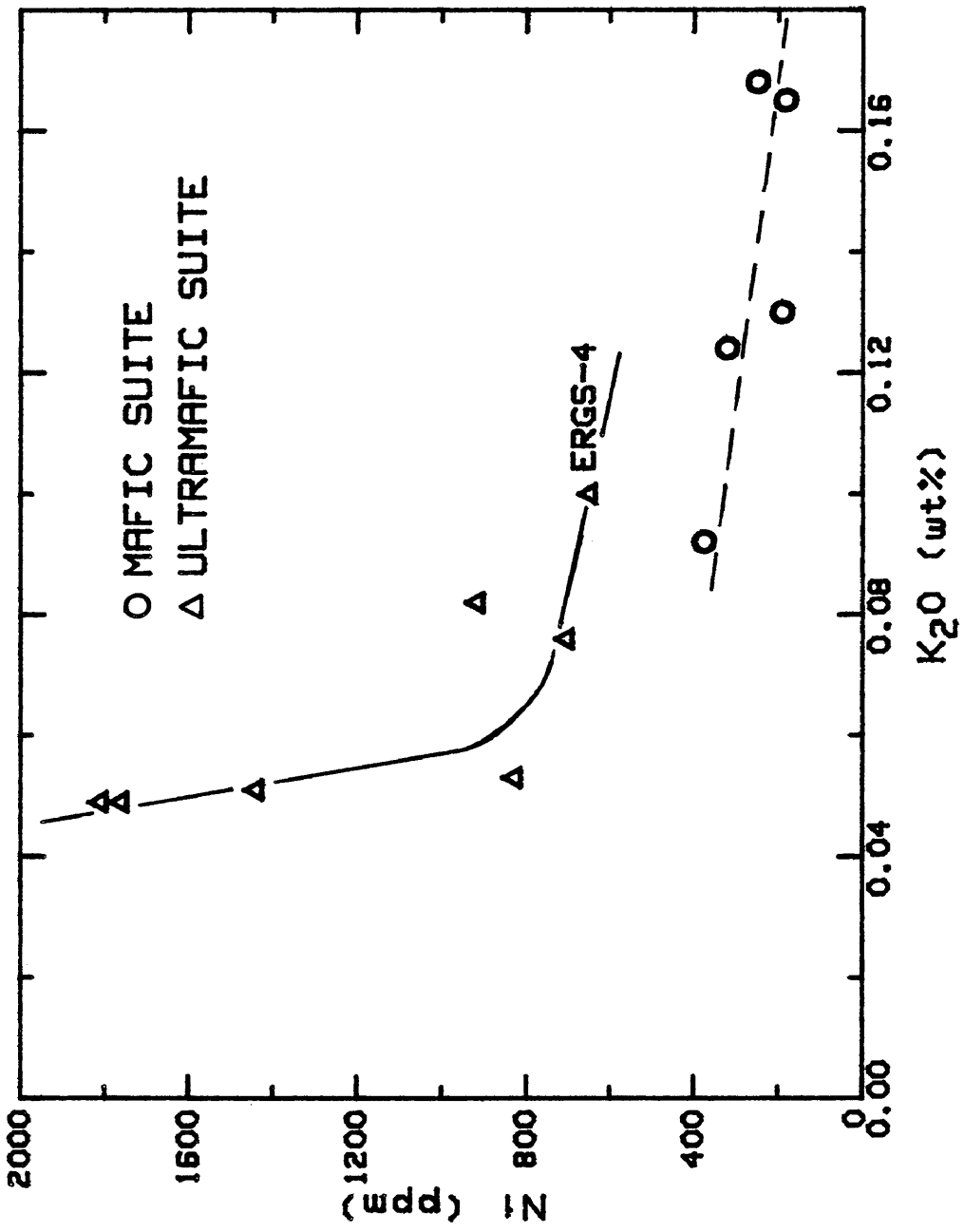
O MAFIC SUITE
Δ ULTRAMAFIC SUITE
Δ ERGS-4
Ni (ppm)
2000
1600
1200
800
400
0
0.00
0.04
0.08
0.12
0.16
K2O (wt%)

Figure 13

clinopyroxene (cpx). As modal cpx decreases, so do abundances of the REE. As mentioned previously, this suggests that the peridotites can be modelled as mixtures of cumulate olivine and opx with variable amounts of "trapped liquid". As the volume% of trapped liquid increases (and thus the modal cpx and plagioclase) so do the $\sum$REE.

The mafic suite has the highest abundances of the REE and also the highest modal% cpx. However, cpx is a major phase in these samples and based on petrographic criteria (fine grain size, equigranular whole-rock), cannot be strictly classified as a "trapped liquid" phase. Sample ERGS-3 has the highest abundances of the REE analyzed and fits well with the less primitive petrographic and major element data of the mafic suite. ERGS-10 could be explained as a plagioclase fractionate of ERGS-3, but for its smaller Eu anomaly when compared to ERGS-3.

Another alternative interpretation of the REE data is that sample ERGS-10 is but a plagioclase-rich fractionate of the peridotite samples. This would give it a higher Ce/Sm ratio than all samples, and, because of removal of olivine and opx, higher REE abundances than cumulate peridotites (ERGS-10 is indeed a plagioclase-rich <u>cumulate</u> segregation from the Cherry Creek Peridotite Body, where

most of the peridotite samples have been collected). In this case ERGS-4 would be the parental magma to all samples analyzed, except ERGS-3. This interpretation would be consistent with the REE data, but does not fit the isotopic data presented earlier (i.e. the greatly differing Nd and Sr isotopes of ERGS-10 from the ultramafic suite).

It is known that a major crust-forming event occurred in Wyoming at between 3.2 to 3.0 Ga, forming a granodioritic crust now represented by the Laramie Granite-Gneiss Terrain in the Laramie Range (Peterman, Z.E., unpublished data). This event would have depleted the upper mantle in the LIL (Large Ion Lithophile) elements. The rising mantle diapir which was melted to form the dikes in the Laramie Range could either have been originally depleted by this event or could have been generated with a chondritic nature, all dependent upon the depth at which the diapir was generated. If the mantle diapir was generated at a relatively shallow depth (as suggested by the Al_2O_3-TiO_2 modelling) then it most likely would have come from a mantle with a depleted signature. Therefore we must take this depletion into account when modelling the evolution of Nd and Sr isotopes in the mantle with time. In successive discussions we will use the depleted upper mantle model of DePaolo (1981) for

Nd isotopes, and that of Peterman (1979) for Sr isotopes. The possibility of this diapir coming from a chondritic source is further refuted when the Nd isotopes are discussed later.

The evolution of Sr in the Laramie Range dikes is shown in Figure 14 along with curves for the evolution of typical upper mantle and upper crust in the Wyoming Province (Mueller, et al, 1985). First note the convergence of samples at about 2.4 to 2.5 Ga, with 5 samples (4 peridotites + 1 mafic suite sample) intersecting the upper mantle curve at this time. Two other samples intersect the upper mantle curve at <3.0 Ga and the remaining samples would intersect this curve at geologically unrealistic ages (these unrealistic ages could be due to multi-stage processes, i.e. small amounts of contamination, or could be an artifact of the author's choice of delpleted mantle model). This convergence suggests a major event at 2.4 to 3.0 Ga, whereby these samples separated from a depleted mantle. Assuming an age for this event of 2.5 Ga (Sm-Nd whole-rock age), the other samples would suggest mixing between an upper crustal component and this depleted mantle, or derivation from a distinctly different source of variable character, such as an Archean lower crust.

Figure 14:

Sr evolution diagram for the ultramafic and mafic dikes from the Laramie Range, Wyoming (Ga = giga-annum or billion years). The solid line is a model upper mantle evolution line and the dash-dot line a model upper crustal evolution line from Peterman (1979). Slopes of the sample lines are determined by present-day $^{87}Rb/^{86}Sr$ ratios of the samples. All samples have the prefix ERGS- .

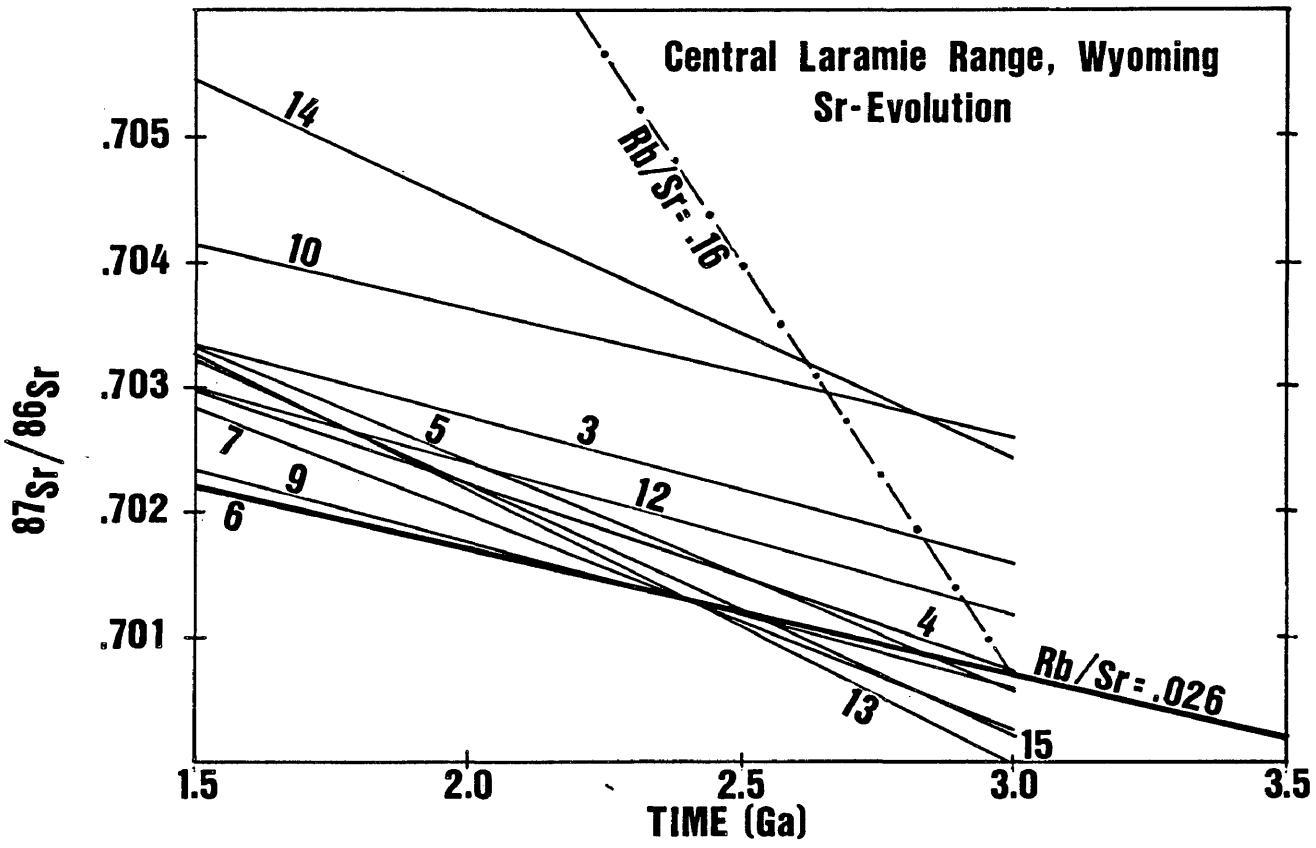
Central Laramie Range, Wyoming
Sr-Evolution
Rb/Sr=.16
Rb/Sr=.026
14
10
7
5
3
9
12
6
4
13
15
.705
.704
.703
.702
.701
87Sr/86Sr
1.5
2.0
2.5
3.0
3.5
TIME (Ga)

Figure 14

Figure 15:

Nd evolution diagram for the ultramafic and mafic dikes from the Laramie Range, Wyoming. The dashed line is a model depleted mantle evolution line (DePaolo, 1981), and the horizontal line at $\epsilon_{Nd} = 0$ is the model chondritic uniform reservoir (CHUR) or bulk earth reference line (DePaolo, 1978). Slopes of the sample lines are determined by present-day values for their respective $^{147}Sm/^{144}Nd$ ratios.

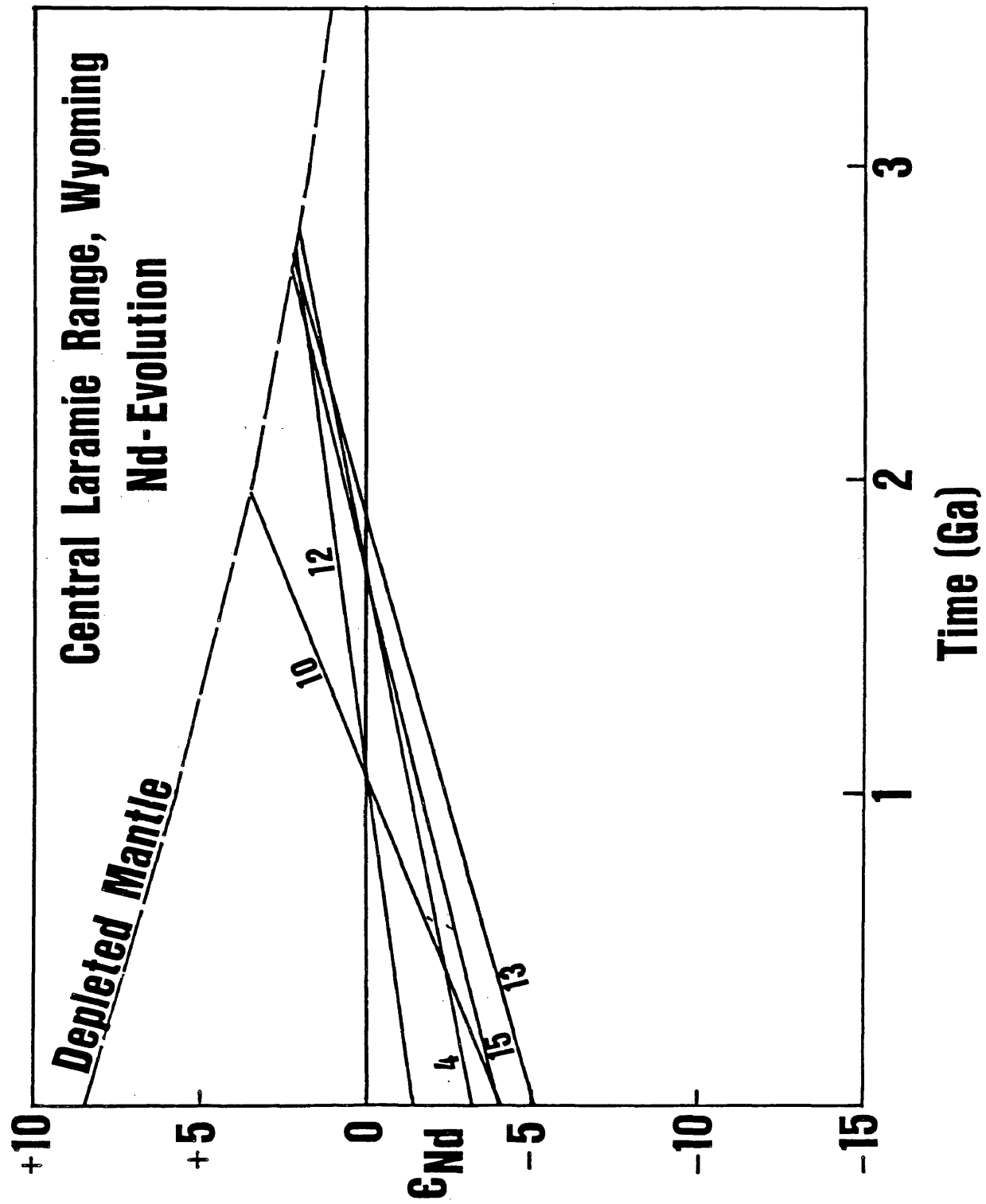
Central Laramie Range, Wyoming
Nd-Evolution
Depleted Mantle
12
10
4
15
13
+10
+5
0
-5
-10
-15
ε_{Nd}
1
2
3
Time (Ga)

Figure 15

The evolution of Nd in the Laramie Range ultramafic samples is shown in Figure 15, along with the model array for the evolution of a depleted mantle. All of the peridotite samples converge quite consistently at ages between 2.5 and 2.7 Ga on the depleted mantle curve. However, one sample of the mafic suite, ERGS-10, crosses the depleted mantle curve at 2.0 Ga. But, we know that sample ERGS-10 comes from within the same body that contains 2 of the peridotites. Therefore, the ages for the peridotites and this sample must be the same (there is no field evidence that ERGS-10 is emplaced either magmatically or tectonically at a later time than the peridotites). If the separation age of 2.5 to 2.7 is valid, then ERGS-10 represents a sampling of the most depleted Archean source region yet analyzed in the literature. The exact location of this region in the asthenosphere-lithosphere is difficult to estimate. Secondly, this sample of a very depleted nature lies within the same intrusion that contains samples of typical depleted mantle. The analysis of this sample has been duplicated by another lab (Dan Unruh, USGS -- Isotope Branch, Denver), and therefore cannot be explained by an analytical faux pax. However, only this one sample has shown this severe depletion.

A second possibility is that the 2.0 Ga separation

age for ERGS-10 is the true age for all of the samples. In this case the other samples from the Laramie Range would give evidence for either a chondritic source or show crustal contamination to varying degrees. Huppert and Sparks (1985) have shown that an ultramafic magma is more likely to be contaminated by lower crust than a more differentiated magma. Therefore it is possible that the peridotites would show evidence of contamination and the mafic suite would show correspondingly less. If contamination were a prevalent mechanism for these samples then the 4-point Sm-Nd isochron given by the peridotites may simply represent a mixing line and may not give a valid age. However, previous discussion (Ni vs. K_2O diagram) has led us to postulate that contamination was not a major process in the evolution of the ultramafic suite (again, unless the contaminant was similar in composition to the ultramafic suite).

If contamination is insignificant, then the evolution of both Nd and Sr with time point to separation of most of these magmas from a depleted upper mantle prior to 2.28 Ga (Sm-Nd whole-rock minimum age, Figure 7) and most probably between 2.4 to 2.6 Ga. The controversy would then arise in that the evolution of Sr suggests the involvement of an enriched source region and the evolution of Nd suggests

involvement of a very depleted component. This dichotomy is evident even within the same sample, ERGS-10.

The contradiction between the Nd and Sr isotopic data for sample ERGS-10 is reconcilable. Though the initial-Nd for this sample suggests a very depleted component, it has the most light-REE enriched pattern of any other sample. This means that the enrichment of this sample must have occurred just prior to or during its separation from the source. At the time of enrichment Rb would also have been elevated, but due to previous multi-stage processes which will be discussed later, this enrichment could have been minor.

Due to the nature of the elements Nd and Sr (as mentioned earlier), during typical earth processes they show fractionations which are negatively coupled. This is due to the fact that during these processes the parent of ^{87}Sr, ^{87}Rb, acts as an incompatible element, whereas the parent of ^{143}Nd, ^{147}Sm, acts as a compatible element. On a plot of ϵ_{Nd} vs. ϵ_{Sr} earth processes typically give trends with a negative slope. Ultramafic rocks in the Laramie Range give a trend with a positive slope. The decoupling of these two systems as shown by our data then suggests a multi-stage process in their genesis.

There are only two instances in the literature known

to the author where a correlation such as this has been documented. One is in a Quaternary volcanic arc succession in central America and (Feigenson, et al, 1986), due to an extremely dissimilar age and tectonic setting, cannot be considered analogous to the ultramafic rocks in the Laramie Range.

The second documented case is from work on anorthosites (Taylor, et al, 1984). Our own work from the Nain Anorthosite Complex (Snyder and Simmons, 1984, and unpublished data) support the observations of Taylor, et al. Typically, anorthosites have very low Rb/Sr and unsupported radiogenic Sr, but both $-\epsilon_{Nd}$ and $+\epsilon_{Nd}$. However, as Taylor, et al point out, all anorthosites are believed to have originated from a depleted source with $+\epsilon_{Nd}$, and crustal residence times determine whether they are positive or negative at the time of emplacement. Proterozoic anorthosite massifs also have light-REE enriched patterns, not dissimilar to ERGS-10.

Like Taylor, et al (1984) we would propose that this sample represents a melt of lower crustal origin. This lower crust was possibly derived from the mantle at 3.2 to 3.0 Ga and subsequently depleted by the melting and extraction of K-granites at 2.7 to 2.6 Ga which make up the Laramie Granite-Gneiss Terrain. This lower crust was then

melted during intrusion of the mantle-derived peridotites, and emplaced within a similar time span between 2.5 to 2.3 Ga. A major unsolved question is whether the lower crust could have a composition which would allow extraction of a felsic melt and still be the source of magmas with 11% MgO and Mg#'s of 0.77. Further studies on the Laramie Granite-Gneiss Terrain and microprobe data on olivines and pyroxenes from samples in this study may help answer this question.

It is interesting to note that the purported tectonic environment of massif-type anorthosites -- incipient or failed rifting -- is similar to that proposed for the central Laramie Range during the late Archean - early Proterozoic.

CONCLUSIONS

Ultramafic and mafic dikes in the central Laramie Range were emplaced in the late Archean - early Proterozoic during a major rifting event. This episode included attenuation of the Archean crust and shallow high percentage melting of the upper mantle beneath the Wyoming Province. Two separate sources for the magmas which formed these rocks have been proposed, along with two separate models. The models for the evolution and melting of these sources are given below :

MODEL I

(1) Development of an extremely heterogeneous mantle beneath Wyoming prior to 2.0 Ga -- one region being depleted, the other retaining a chondritic nature.

(2) Melting of both source regions at 2.0 Ga to give a suite of samples with nearly chondritic REE patterns and C_{Nd} near zero, and a suite with slightly light-REE enriched patterns and ϵ_{Nd} of +4 (Figure 16).

This model fails to explain the Sr isotopic data, which could possibly have been altered by later amphibolite facies metamorphism in this region. It also fails to comply with the Sm-Nd whole-rock isochron which gives a minimum age of 2.28 Ga. However, this age could then be interpreted as the artifact of a simple mixing line between

Figure 16:

Nd evolution diagram for Model I as described in the text. DM = depleted mantle (DePaolo, 1981), BE = bulk earth or chondritic uniform reservoir (DePaolo, 1978), M = mafic suite evolution line, UM = ultramafic suite evolution array.

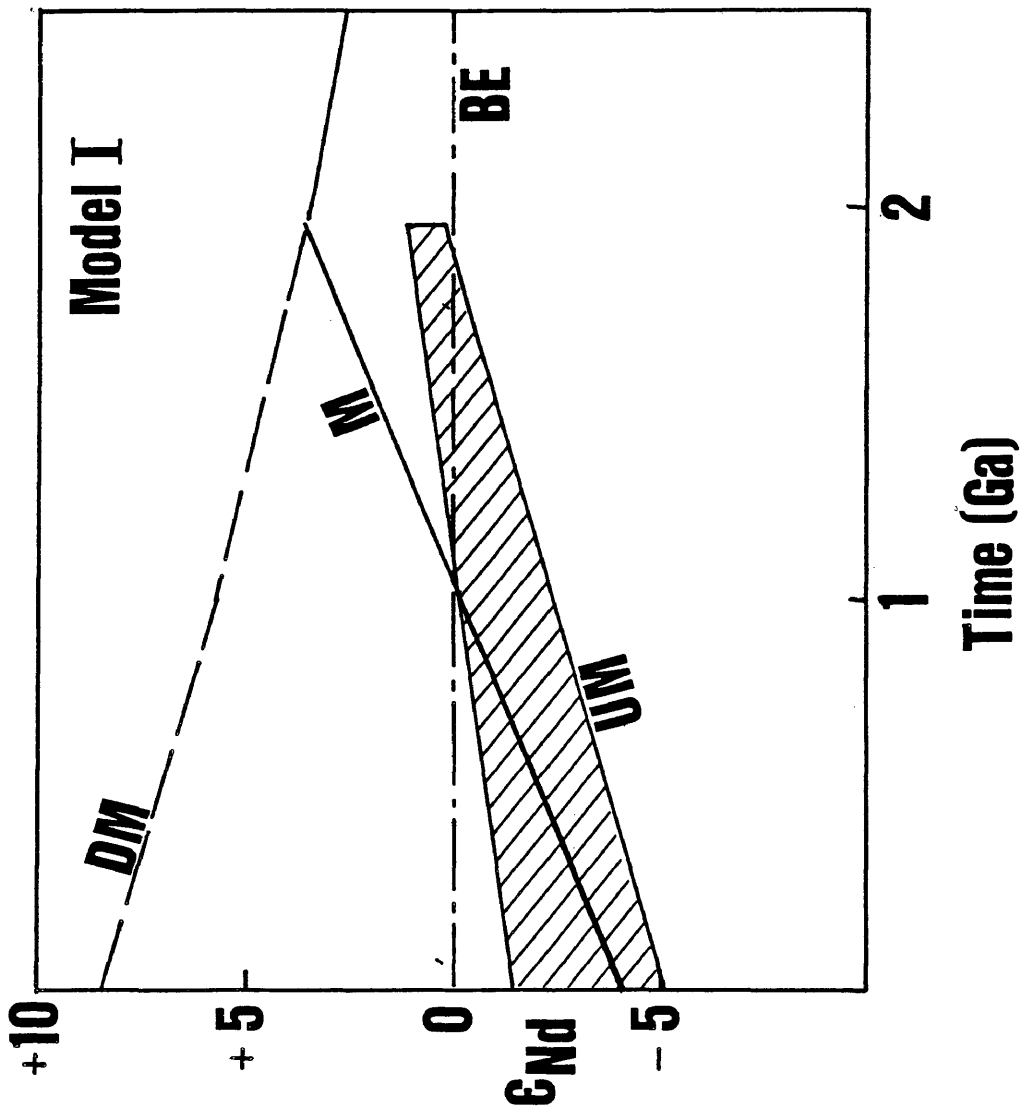

Figure 16

two different sources, one chondritic and the other depleted in nature.

Assuming that the Sr isotopic data can be used effectively to determine source characteristics and the Sm-Nd isochron gives a true age, then the following model is preferred (Figures 17 and 18):

MODEL II

(1) A granodiorite/tonalite Archean crust was formed at 3.2 to 3.0 Ga, depleting the mantle in the LIL elements. The Archean crust at this time had an extremely high Rb/Sr ratio and relatively low, though less fractionated, Sm/Nd.

(2) K-rich granites were generated at 2.7 to 2.6 Ga by partial melting of the Archean lower crust, thus depleting the lower crust in K and Rb and enriching it in Sm. Thus, the lower crust at this time had low Rb/Sr and high Sm/Nd. The absolute value of the fractionation of Sm/Nd relative to the Sm/Nd for the depleted mantle must be greater in this process than that in the previous fractionation event (Figure 17)*. Only if this is true would the Nd in the lower crust retain a more depleted signature than that of the depleted mantle.

(3) Rifting, attenuation of the Archean crust, and intrusion of melts derived directly from the upper mantle occurs (forming the ultramafic suite). Thinning of the

Figure 17:

Nd evolution for Model II as described in the text. The numbers 1, 2, and 3 correspond to those in the text. DM = depleted mantle (DePaolo, 1981), BE = bulk earth. For simplicity only the evolution of the mafic suite is shown.

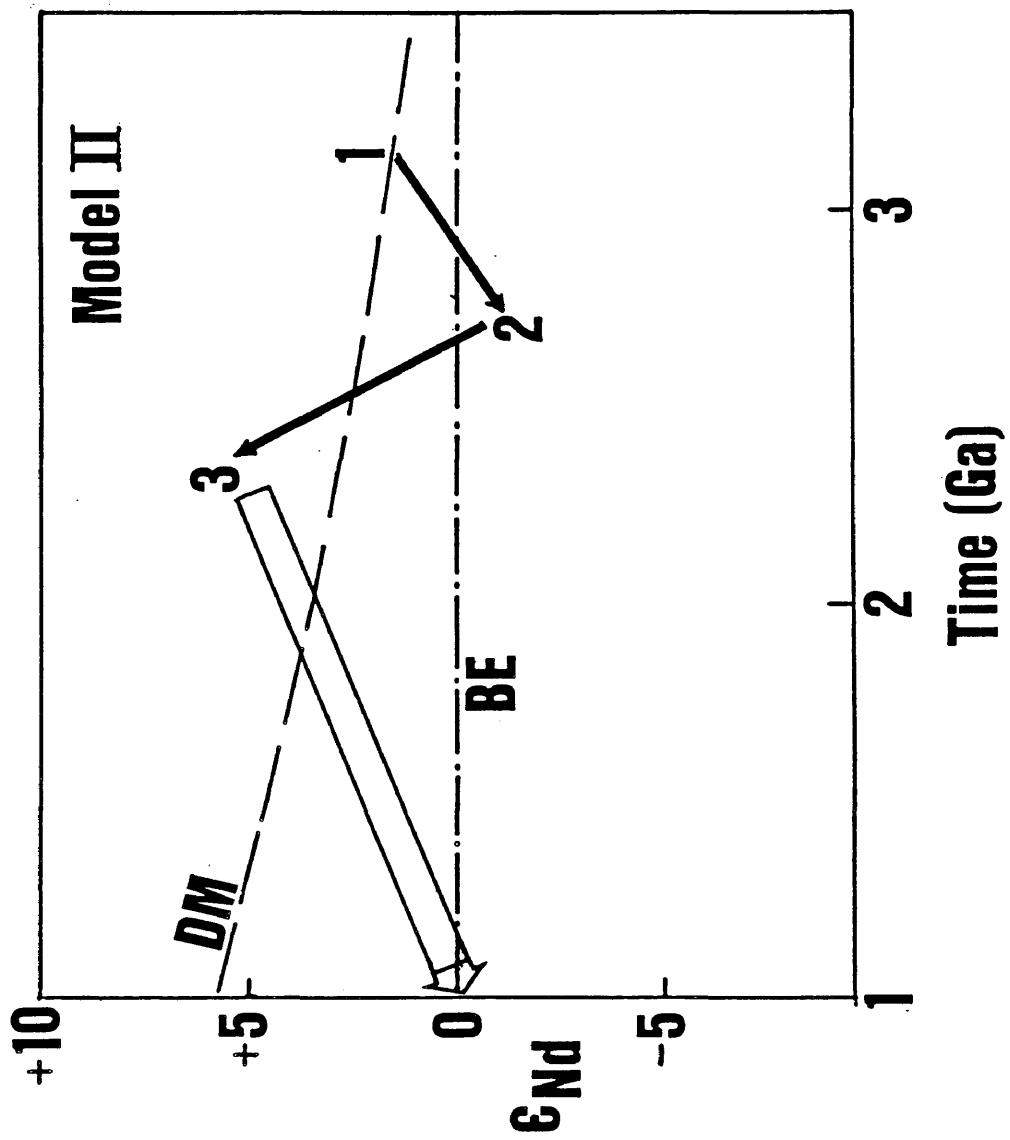

Figure 17

Figure 18:

Cartoon of Model II showing the geologic processes invisioned by the author in the evolution of the crust and mantle under the central Laramie Range between 3.2 and 2.5 Ga, and the subsequent intrusion of the ultramafic and mafic dike suites. A, B, and C correspond to 1, 2, and 3, respectively, in the text. See text for explanation.

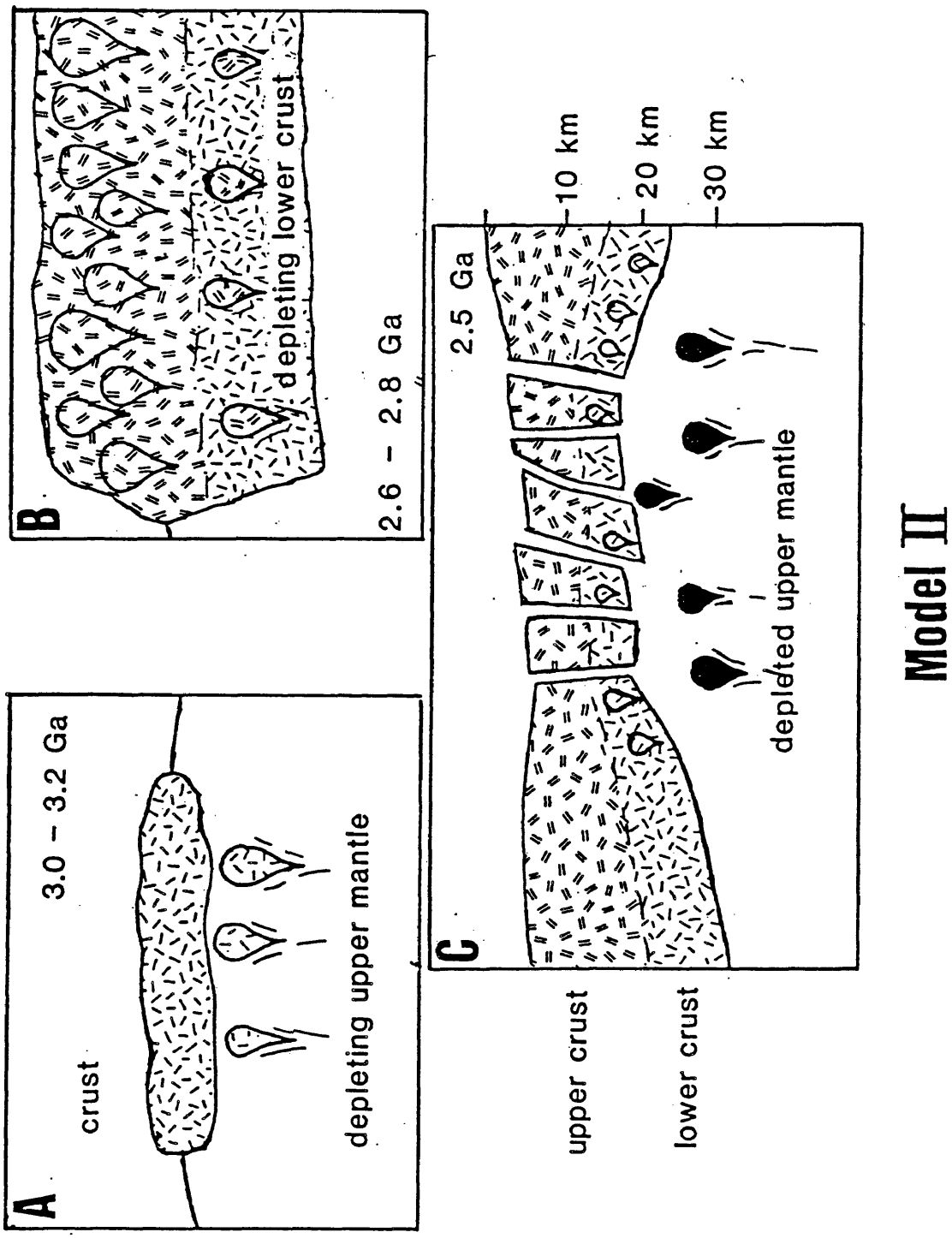
A
3.0 - 3.2 Ga
crust
depleting upper mantle
B
2.6 - 2.8 Ga
depleting lower crust
C
2.5 Ga
10 km
20 km
30 km
upper crust
lower crust
depleted upper mantle
Model II

Figure 18

crust and intrusion of the ultramafic magmas raises the temperature of the lower crust to approximately 1300°C (Taylor, et al, 1984, and plot of mafic suite on FeO-MgO plot, Figure 10) and melts mafic portions of the lower crust which are subsequently intruded. These lower crustal melts have relatively low Rb/Sr ratios and high $^{87}Sr/^{86}Sr$ compared to the mantle melts and light-REE enriched patterns, but depleted ϵ_{Nd} values due to its residence time in the Archean lower crust with a high Sm/Nd.

---

*i.e., {$f^{Sm/Nd}$(DM) for process 1} < {$f^{Sm/Nd}$(DM) for process 2}, where $f^{Sm/Nd}$(DM) is defined similar to DePaolo's notation (1978), but uses his depleted mantle model (DePaolo, 1981) instead of the chondritic uniform reservoir as a reference point:

$$f^{Sm/Nd} = \frac{(Sm/Nd)_{rock}}{(Sm/Nd)_{depl.\ mantle}} - 1$$

REFERENCES CITED

Abbey, S., 1983, Studies in "standard samples" of silicate rocks and minerals, 1969-1982: Canada Geological Survey Paper 83-15, 114pp.

Campbell, I.H., 1985, The difference between oceanic and continental tholeiites: a fluid dynamic explanation: Contrib. Mineral. Petrol., v. 91, p. 37-43.

Cawthorn, R.G. and Davies, G., 1982, Possible komatiitic affinity of the Bushveld Complex, South Africa, in N.T. Arndt and E.G. Nisbet, editors, Komatiites: George Allen & Unwin, London, p. 91-96.

Cawthorn, R.G., Davies, G., Clubley-Armstrong, A., and McCarthy, T.S., 1981, Sills associated with the Bushveld Complex, South Africa: an extimate of the parental magma composition: Lithos, v. 14, p. 1-15.

DePaolo, D.J., 1978, Study of magma sources, mantle structure and the differentiation of the earth from variations of $^{143}Nd/^{144}Nd$ in igneous rocks: Unpublished Ph.D. thesis, Calif. Instit. Tech., 360 pp.

DePaolo, D.J., 1979, Implications of correlated Nd and Sr isotopic variations for the chemical evolution of the crust and mantle: Earth Planet. Sci. Lett., v. 43, p. 201-211.

DePaolo, D.J., 1981, Neodymium isotopes in the Colorado Front Range and crust-mantle evolution in the Proterozoic: Nature, v. 291, p. 193-196.

DePaolo, D.J. and Wasserburg, 1976, Nd isotopic variations and petrogenetic models: Geophys. Res. Lett., v. 3, p. 249-252.

Divis, A.F., 1976, Geology and geochemistry of Sierra Madre Range, Wyoming: Colo. Sch. Mines Quart., v. 71, no. 3, 127 pp.

Divis, A.F., 1977, Isotopic studies on a Precambrian geochronologic boundary, Sierra Madre Mountains, Wyoming: Geol. Soc. Amer. Bull., v. 88, p. 96-100.

Feigenson, M.D. and Carr, M.J., 1986, Positively correlated Nd and Sr isotope ratios of lavas from the Central American volcanic front: Geology, v. 14, p. 78-82.

Frey, F.A., Suen, C.J., and Stockman, H.W., 1985, The Ronda high temperature peridotite: geochemistry and petrogenesis: Geochim. Cosmochim. Acta, v. 49, p. 2469-2491.

Graff, P.J., Sears, J.W., Holden, G.S., and Hausel, W.D., 1982, Geology of the Elmer's Rock Greenstone Belt, Laramie Range, Wyoming: Geol. Surv. Wyom., Rept. Invest. 14, 23 pp.

Hanson, G.N., 1980, Rare earth elements in petrogenetic studies of igneous systems: Ann. Rev. Earth Planet. Sci., v. 8, p. 371-406.

Hanson, G.N. and Langmuir, C.H., 1978, Modelling of major elements in mantle-melt systems using trace element approaches: Geochim. Cosmochim. Acta, v. 42, p. 725-741.

Heimlich, R.A. and Banks, P.O., 1968, Radiometric age determinations, Bighorn Mountains, Wyoming: Amer. Jour. Sci., v. 266, p. 180-192.

Heinrich, E.W., 1965, Microscopic Identification of Minerals: McGraw Hill, Inc., New York, 414 pp.

Hills, F.A. and Armstrong, R.L., 1974, Geochronolgy of Precambrian rocks in the Laramie Range and implications for the tectonic framework of Precambrian southern Wyoming: Precamb. Res., v. 1, p. 213-225.

Hills, F.A., Gast, P.W., Houston, R.S., and Swainbank, I.G., 1968, Precambrian geochronology of the Medicine Bow Mountains, southeastern Wyoming: Geol. Soc. Amer. Bull., v. 79, p. 1757-1784.

Hills, F.A. and Houston, R.S., 1979, Early Proterozoic tectonics of the central Rocky Mountains, North America: Contr. Geol., Univ. Wyo., v. 17, p. 89-109.

Holden, G.S. and Snyder, G.L., 1983, Compositional variation of mafic rocks from an Archean granite-greenstone terrane, central Laramie Range, Wyoming: Geol. Soc. Amer. Abstr. w. Prog., v. ?.

Hughes, C.J., 1982, Igneous Petrology: Elsevier Sci. Publishing Co., Amsterdam, 551 pp.

Huppert, H.E. and Sparks, R.S.J., 1985, Cooling and contamination of mafic and ultramafic magmas during ascent through continental crust: Earth Planet. Sci. Lett., v. 74, p. 371-386.

Irvine, T.N., 1982, Terminology for layered intrusions: Jour. Petrol., v. 23, p. 127-162.

Jahn, B.-M., Bernard-Griffiths, J., Charlot, R., Cornichet, J., and Vidal, F., 1980, Nd and Sr isotopic compositions and REE abundances of Cretaceous MORB (holes 417D and 418A, Legs 51, 52, and 53): Earth Planet. Sci. Lett., v. 48, p. 171-184.

Jaques, A.L. and Green, D.H., 1980, Anhydrous melting of peridotite at 0-15 kb pressure and the genesis of tholeiitic basalts: Contrib. Mineral. Petrol., v. 73, p. 287-310.

Jensen, L.S., 1976, A new cation plot for classifying subalkalic volcanic rocks: Ontario Div. Mines Misc. Paper 66, 22 pp.

Johnson, R.C. and Hills, A.F., 1976, Precambrian geochronology and geology of the Boxelder Canyon area, northern Laramie Range, Wyoming: Geol. Soc. Amer. Bull., v. 87, p. 809-817.

Karlstrom, K.E. and Houston, R.S., 1984, The Cheyenne Belt: analysis of a Proterozoic suture in southern Wyoming: Precamb. Res., v. 25, p. 415-446.

Lambert, D.D., 1982, Geochemical evolution of the Stillwater Complex, Montana: evidence for the formation of platinum-group element deposits in mafic layered intrusions: Unpublished Ph.D. thesis, Colo. Sch. Mines, 274 pp.

Longhi, J., Wooden, J.L., and Coppinger, K.D., 1983, The petrology of high-Mg dikes from the Beartooth Mountains, Montana: a search for the parent magma of the Stillwater Complex: Proc. 14th Lunar Planet. Sci. Conf., Jour. Geophys. Res. 88, suppl., p. B53-B69.

Ludwig, K.R., 1982, User's guide to DBAT1B -- a computer program for operation of a Micromass 54E mass-spectrometer: U.S. Geol. Surv. Open-file Report 82-1079, 50 pp.

Ludwig, K.R., 1985, User's manual for ANALYST, a computer program for control of an Isomass 54E thermal-ionization, single-collector mass-spectrometer: U.S. Geol. Surv. Open-file Report 85-141, 89 pp.

Ludwig, K.R. and Stuckless, J.S., 1978, Uranium-lead isotope systematics and apparent ages of zircons and other minerals in Precambrian granitic rocks, Granite Mountains, Wyoming: Contrib. Mineral. Petrol., v. 65, p. 241-254.

Lugmair, G.W., 1974, Sm-Nd ages: a new dating method: Meteoritics, v. 9, p. 369.

Mueller, P.A., Peterman, Z.E., and Granath, J.W.,

1985, A bimodal Archean volcanic series, Owl Creek Mountains, Wyoming: Jour. Geol., v. 93, p. 701-712.

Naylor, R.S., Steiger, R.H., and Wasserburg, G.J., 1970, U-Th-Pb and Rb-Sr systematics in 2700 x 10^6 years old plutons from the southern Wind River Range, Wyoming: Geochim. Cosmochim. Acta, v. 34, p. 1133-1150.

Nelson, B.K. and DePaolo, D.J., 1984, 1700-Myr greenstone volcanic successions in southwestern North America and isotopic evolution of Proterozoic mantle: Nature, v. 311, p. 143-146.

Nelson, B.K. and DePaolo, 1985, Rapid production of continental crust 1.7 to 1.9 b.y. ago: Nd isotopic evidence from the basement of the North American mid-continent: Geol. Soc. Amer. Bull., v. 96, p. 746-754.

Ohtani, E., 1984, Generation of komatiite magma and gravitational differentiation in the deep upper mantle: Earth Planet. Sci. Lett., v. 67, p. 261-272.

O'Nions, R.K., Hamilton, P.J., and Evensen, N.M., 1977, Variations in $^{143}Nd/^{144}Nd$ and $^{87}Sr/^{86}Sr$ ratios in oceanic basalts: Earth Planet. Sci. Lett., v. 34, p. 13-22.

Palmer, M.R. and Elderfield, H., 1985, Sr isotope composition of sea water over the past 75 Myr: Nature, v. 314, p. 526-528.

Peterman, Z.E., 1979a, Strontium isotope geochemistry of late Archean to late Cretaceous tonalites and trondhjemites, in F. Barker, editor, Dacites, Trondhjemites, and Related Rocks: Elsevier Sci. Publ. Co., Amsterdam, p. 133-147.

Peterman, Z.E., 1979b, Geochronology and the Archean of the United States: Econ. Geol., v. 74, p. 1544-1562.

Peterman, Z.E. and Hildreth, R.A., 1978, Reconnaissance geology and geochronology of the Precambrian of the Granite Mountains, Wyoming: U. S. Geol. Surv. Prof. Paper 1055, 22 pp.

Potts, M.J., 1972, Origin of a Precambrian ultramafic intrusion in southeastern Wyoming, U.S.A.: Contrib. Mineral. Petrol., v. 36, p. 249-264.

Shirey, S.B., 1984, Origin of the Archean crust in the Rainy Lake Area, Ontario: Unpublished Ph.D. thesis, SUNY Stony Brook, 393 pp.

Sims, P.K. and Peterman, Z.E., 1986, Early Proterozoic Central Plains orogen: a major buried structure in the north-central United States: Geology, v. 14, p. 488-491.

Snyder, G.A. and Simmons, E.C., 1984, Preliminary Nd isotope data from the Goodnews Complex, Labrador: evidence for the existence of two magma series (abstract): Trans. Amer. Geophys. Union, v. 65, p. 305.

Snyder, G.L., 1984, Preliminary geologic maps of the central Laramie Mountains, Albany and Platte Counties, Wyoming: U. S. Geol. Surv. Open File Rept. 84-358 (A-M), 15 pp. of text.

Steiger, R.H. and Jager, E., 1977, Subcommission on geochronology -- convention on the use of decay constants in geo- and cosmo-chronology: Earth Planet. Sci. Lett., v. 36, p. 359-362.

Stille, P. and Clauer, N., 1986, Sm-Nd isochron-age and provenance of the argillites of the Gunflint Iron Formation in Ontario, Canada: Geochim Cosmochim. Acta, v. 50, p. 1141-1146.

Streckeisen, A.L. (chairman), 1973, Plutonic rocks: classification and nomenclature recommended by the IUGS subcommission on the systematics of igneous rocks: Geotimes, v. 18, p. 26-30.

Stuckless, J.S., Hedge, C.E., Worl, R.G., Simmons, K.R., Nkomo, I.T., and Wenner, D.B., 1985, Isotopic studies of the late Archean plutonic rocks of the Wind River Range, Wyoming: Geol. Soc. Amer. Bull., v. 96, p. 850-860.

Subbarayudu, G.V., Hills, F.A., and Zartman, R.E., 1975, Age and Sr isotopic evidence for the origin of the Laramie Anorthosite-Syenite Complex, Laramie Range, Wyoming (abstract): Geol. Soc. Amer. Abstr. w. Prog., v. 7, p. 1287.

Sun, S.-S., 1984, Geochemical characteristics of Archean ultramafic and mafic volcanic rocks: implications for mantle composition and evolution, in A. Kroner, et al, editors, Archean Geochemistry: Springer-Verlag, Berlin, 300 pp.

Taylor, S.R., Campbell, I.H., McCulloch, M.T., and McLennan, S.M., 1984, A lower crustal origin for massif-type anorthosites: Nature, v. 311, p. 372-374.

Theobald, P.K. and Thompson, C.E., 1968, Platinum and associated elements at the New Rambler Mine and vicinity Albany and and Carbon Counties, Wyoming: U.S. Geol. Surv. Circ. 607, 14 pp.

Wasserburg, G.J., Jacobsen, S.B., DePaolo, D.J., McCulloch, M.T., and Wen, T., 1981, Precise determinations of Sm/Nd ratios, Sm and Nd isotopic abundances in standard solutions: Geochim. Cosmochim. Acta, v. 45, p. 2311-2323.

Watson, E.B. and Jurewicz, S.R., 1984, Behavior of alkalies during diffusive interaction of granitic xenoliths with basaltic magma: Jour. Geol., v. 92, p. 121-131.

Weaver, B.L. and Tarney, J., 1984, Empirical approach to estimating the composition of the continental crust: Nature, v. 310, p. 575-577.

APPENDIX I -- ANALYTICAL PROCEDURES

Sample Collection and Grinding

Five to ten kg samples were collected in the field and weathering rinds were chipped off on location. Samples were collected in canvas sample bags, numbered, and brought out for grinding. Grinding was completed mostly by hand. First, samples were reduced to 1-2 cm. chips with a hand sledge and a steel plate. The full sample was then run through a mechanical splitter, until only a quarter of the sample remained. This was then mixed by hand on a large piece of butcher paper (4 ft. x 4 ft.) for 40 minutes to obtain a homogeneous mixture. The mixing is accomplished by carefully lifing a corner of the paper and turning it over until it meets the opposing corner. The sample must not be allowed to slide along the paper, but must fall off of the upper paper onto the lower. The process is then continued with another corner of the paper until the time has elapsed. The sample was then collected into a symmetric pile and quartered using a large spatula. Two diagonally opposing quarters were saved for further mixing, the other pair of quarters was returned to the rest of the sample.

This process was continued until approximately 1/4 kg

of sample remained. This portion of the sample was then ground in a stainless steel mortar and pestle to a sand-sized grit. The sample was again mixed on butcher paper, quartered, and split until approximately 50 g of sample remained. The 50 g fraction was then ground to <-80 mesh in an agate mortar and pestle. Once the complete fraction has been passed through an 80-mesh sieve, the whole was then ground mechanically for 10 minutes in a stainless steel ball-mixer. This insured that the sample was -200 mesh in grain size. The sample was placed in a plastic vial with air-tight seal cap, ready for dissolution. The -200 mesh is important once the final vial is mixed. This grain size is such that electrostatic charges keep the grains from settling due to density differences, and thus the "representative whole-rock" integrity of the sample is maintained without further mixing.

Preparation of Fused Discs for Major Element Analyses

The whole-rock samples are dried in an oven at 115°C for 10-16 hours. Precisely 0.5000 g of whole-rock powder was then weighed into a cleaned and tared glass vial. Precisely 4.5000 g of lithium tetraborate flux was then added to the same vial. The two compounds were then

mixed mechanically on a wheel for 2-4 hours.

Drying experiments were performed on the batch of flux used in our labs at CSM. It was found that drying of the flux at 125^{o} for 20 hours will drive off most, if not all occluded water. The water content of the lot of flux (Spex Industries, lot# 01851R) used is approximately 2.8%. Drying of the flux is necessary to insure an exact 9:1 mixture, by mass, of flux:sample (to allow for consistent matrix corrections on the XRF), and to simplify the melting of the mixture (Joe Taggert, USGS, personal communication).

To this mixture is then added 3-5 drops of a 10% LiI solution and is subsequently melted in 95% Pt-5% Au crucible over a natural gas- oxygen flame for 15-20 minutes until it is homogeneous in appearance. The melt is then quickly poured into a 95% Pt-5% Au pan which has been heated to red hot by a natural gas- air flame (this decreases the number of bubbles in the disc markedly). The melt and pan are then allowed to cool to room temperature. The fused disc is then tapped gently out of the pan, allowing nothing to touch the analytical surface.

When heated to redness, the crucibles and pans are handled only with Pt-tipped tongs. The crucibles are cleaned by immersion in a warm (80^{o}C) 6N HCl bath, rinsing with 3xH_2O and flame-drying. The pans are rinsed

with 2N HCl and then 3xH_2O and also flame-dried. To maintain the integrity of the surface, the bottom, or analytical surface of the pans must never be touched or dried with a kim-wipe.

The discs should be perfectly clear (though they are generally colored) with no imperfections and few, if any, bubbles. The analytical surface should be perfectly flat. With time, the pans begin to warp and must be periodically be re-pressed in their molds (about every 100-150 discs made).

The discs were analyzed on a Rigaku X-ray Flourescence Spectrometer (XRF) using the program S-MAX (Carl Eriksson, personal communication, 1985). Precision for the major elements was determined through duplicate analyses of all samples and is generally less than 1%, relative (with the exception of TiO_2, <2%, Fe_2O_3, <2%, Na_2O, <20%, and P_2O_5, <6%). Accuracy, as determined by analyzing 34 standard rock samples and performing regression analyses for each oxide using the sub-routine XRF-CAL are given in Table IA as % absolute. Standard rock samples were also analyzed by the author and are shown in Table IB along with accepted literature values from Abbey (1983). All of the major elements (and Ni) for the standards analyzed show reasonable accuracy when

Table IA

Major Element Accuracy, in Weight % Absolute

(95 % confidence level)

Oxide	% Absolute
SiO_2	0.41
TiO_2	0.026
Al_2O_3	0.24
Fe_2O_3	0.22
MnO	0.006
MgO	0.14
CaO	0.066
Na_2O	0.063
K_2O	0.032
P_2O_5	0.010

Table IB

Rock Standards (Anhydrous): Major Elements

	DTS-1			BHVO-1		
	Abbey*	1	2	Abbey	1	2
SiO_2	40.61	40.37	40.11	49.90	49.45	49.03
TiO_2	0.00	0.01	0.00	2.69	2.71	2.69
Al_2O_3	0.25	0.31	0.33	13.85	13.75	13.65
$Fe_2O_3^T$	8.73	8.81	8.60	12.24	12.17	12.26
MnO	0.12	0.11	0.11	0.17	0.17	0.17
MgO	49.80	50.04	49.64	7.31	7.31	7.33
CaO	0.14	0.10	0.10	11.33	11.37	11.38
Na_2O	0.01	0.00	0.10	2.29	2.15	2.24
K_2O	0.00	0.02	0.02	0.54	0.53	0.54
P_2O_5	0.00	0.01	0.01	0.28	0.27	0.27
Total	99.66	99.78	99.02	100.60	99.88	99.56
Ni(ppm)**	2300	2340	2240			

* Values from Abbey (1983).

^{T} Total Fe as Fe_2O_3, as measured directly on the XRF. Values from Abee recalculated using the following equation, $Fe_2O_3^T = 1.1111 \times FeO + Fe_2O_3$.

** Our values were analyzed by Atomic Absorption Spectrometry.

compared to the literature values of Abee, except SiO_2, which is consistently low by 1.1%. Large errors are found in DTS-1 for Na_2O, K_2O, and P_2O_5 due to the small amounts of the oxides in this standard. Errors of this magnitude are not seen in these oxides for BHVO-1. The standards DTS-1 (dunite) and BHVO-1 (Hawaiian basalt) were used because they cover both ends of the major element spectrum found in the samples analyzed in this study.

Loss on ignition (LOI) was determined by weighing a known amount of whole-rock sample into a porcelain crucible and heating the sample in a muffle furnace for 45 minutes at 1000°C. The crucibles were then placed in a dessicator and allowed to cool to room temperature (1-2 hours). The sample was weighed, with the difference between the first and second weighings giving the LOI.

To obtain LOI in weight %, divide this difference by the weight of the sample before heating and multiply by 100. If the sample loses weight, the LOI is reported positive, but if the sample gains weight it is reported negative. To this figure is then added a factor which takes into account the oxidation of Fe from the +2 to +3 state, and thus the addition of weight due to the addition of O_2 to the sample. Multiply 0.111348 times the weight % FeO in the sample and add this to the initial LOI value,

to give the true LOI.

Sample Dissolution

From 100 to 500 mg of sample were weighed on a single-pan mechanical balance into clean acid-washed Savillex (brand) teflon "bombs". 5 ml of 6 N HNO_3 was then added, the bomb sealed, and the acid allowed to react with any organics in the sample for 10-15 minutes. At this point spikes for isotope dilution would be added. The mixture was then placed on a hot plate at 90°C until only a small amount of liquid remained.

At this point 2 ml of HF and 1 ml of $HClO_4$ was then added for initial dissolution. The bomb was sealed and the contents were allowed to digest for 24 hours at 70°C. The bomb was then opened, allowing a large portion of the silicon in the sample to be driven off as SiF_4 gas. Approximately 3 ml of HF and a few drops of $HClO_4$ were then added to the bombs. The bombs were sealed and, depending upon the sample size and composition, left on the hot plate at 70°C for 3-6 days. The samples were again opened and heated to 90°C to allow the remaining silicon to be fumed off as SiF_4 gas. At this point the samples were allowed to be heated to complete dryness. This may take 1-2 days at 90°C due to the high vaporization

temperature of $HClO_4$, but is necessary to insure that no HF remains (it will etch glassware used in successive steps).

The sample is then brought into solution in 10-15 ml of 6 N HCl. The bombs must be checked thoroughly that all of the sample has been dissolved, with no residue remaining. Heating samples at 50-60°C in the sealed bomb with 6 N HCl will insure complete dissolution. Once dissolution is complete, and all spikes have been equilibrated with 100% of the sample, the sample is again taken to dryness. The sample is now ready to be loaded onto an elution column in the solution suited for that column.

It is important to note that often only 1-2 ml of a somewhat dilute acid is used for loading samples on an elution column. This means that all of the sample will not be dissolved in the loading solution. Therefore, centrifuging of samples is necessary so that residues will not be inadvertently poured onto the columns. Residues in the column could be slowly dissolved during the elution, causing elements to be released continuously throughout the elution and destroying any separation of elements one may have hoped for. That a small amount of residue remains in the loading fraction is not significant (as long as it does

not go on the column), provided that at one point the spikes have been dissolved and equilibrated with 100% of the sample, as stated above. Though some of the element desired may be lost in the residue, there is no evidence that isotope fractionation occurs during separation of an insoluble phase; indeed, the reproducibility of standards supports the opposite.

Separations Chemistry

I. The elements Rb and Sr

The elements Rb and Sr are analyzed for isotopic work. Rb was analyzed for abundance data only, and Sr for both abundance data and isotopic composition. Since Rb and Sr mutually interfere at mass 87, a quantitative separation of the two must be effected through ion exchange column chemistry.

Rb and Sr are crudely separated from other cations through a first elution pass on a polypropylene Bio-Rad column (8 mm I.D. x 11 ml vol., with 1.8 ml of Dowex AG-50Wx12 cation exchange resin) using 4 N HCl as the elluent. Rb is then added onto a final polypropylene column (same dimensions and resin) and eluted with 0.5 N HCl to effect a complete separation of Rb from Sr.

Sr is then added onto a 0.4 x 14 cm "champagne-glass"

column which gives a superb separation of Sr from Rb and Ca (Min, 1986). Formerly, the polypropylene columns were used for further separation of Sr, but two passes were needed to give a clean Sr fraction and Ca was still an intermittent problem. The interference of Ca (which affects the ionization efficiency and stability of Sr during thermal ionization on the mass spectrometer) was completely eliminated by the "champagne-glass" columns due to a greater aspect ratio (length or volume of the resin over the inner diameter of the column) of these columns.

Both Rb and Sr fractions are then dried down at a temperature of 80°C in 5 ml teflon beakers and are wrapped in Parafilm plastic wrap for transportation to the USGS--Isotope Branch for analysis.

II. The Rare Earth Elements

In general the separation scheme for the REE is given in Lambert (1982), and therefore will not be covered here. However, one modification has been made in the procedure. Initial group separation of the REE is accomplished on a 1 x 20 cm glass column filled with AG-50Wx8 (200-400 mesh) cation exchange resin. A column of this size was needed to give a relatively clean separation and avoid overloading due to large sample sizes used in this study (400-500 mg).

The resin was rinsed several times with 200ml of 6 N HCl and then equilibrated in 1 N HCl. The sample of interest is then loaded in 15ml of 1 N HCl onto the column and rinsed several times with 1-2 ml of dilute HCl (0.5-1 N). The elution procedure is given in Crock (1984) and below:

(1) elute 50ml 2 N HCl and discard (contains Fe)

(2) elute 70ml 2 N HNO_3 and discard

(3) elute 70ml 6 N HNO_3 and collect for REE.

The REE fraction is then dried down on a hot plate and loaded onto the 0.5 x 10 cm columns (1.31 ml of resin) used in Lambert (1982).

Isotope dilution Sm-Nd ratios obtained in the analyses of the REE were used in calculating $^{147}Sm/^{144}Nd$ and to determine initial ratios in Nd isotopic studies.

III. The Element Nd (for isotopic composition)

Because of the interference of ^{144}Sm on the normalizing isotope of Nd, ^{144}Nd, a precise, highly quantitative separation must be made of Sm from Nd. There are many semi-quantitative methods for separation of individual rare-earth elements, but not until 1970 was a quantitative method used in isotopic analyses (Eugster, et al, 1970). This method was used in 1974 to pioneer the

analysis of Nd isotopes in geochemical samples (Lugmair, 1974). In the past ten years several new methods have been developed for chemical separation of Sm from Nd for Nd isotopic analysis, but the method described herein is a modification of the first. For further information on Nd separations chemistry beyond the scope of this work see Shirey (1984) or DePaolo (1978).

Depending upon the size of the sample to be analyzed, two different sets of preliminary column passes are used at CSM. For samples <100 mg in size the following procedure is used:

Column I (0.8 cm I.D. x 11 ml vol., Bio-Rad, with 1.8 ml of AG50Wx12, 200-400 mesh cation resin).

(1) equilibrate column in 4 N HCl
(2) load sample onto resin in 1 ml 4 N HCl
(3) wash column with 0.5 ml 1 N HCl
(4) elute 7 ml 4 N HCl --> discard
(5) elute 12 ml 4 N HCl --> collect for Nd
(6) dry down this sample at 200°C

Column II (same column as above with AG50Wx8, 200-400 mesh, cation resin; modified from Jahn, 1980)

(1) equilibrate column in 2 N HCl
(2) load sample onto resin in 1 ml 1 N HCl

(3) elute 8 ml of 2 N HCl --> discard

(4) rinse column with 1.5 ml triple-distilled H_2O ($3x H_2O$) --> discard

(5) elute 17 ml 2 N HNO_3 --> discard

(6) elute 18 ml 2 N HNO_3 --> collect for Nd

(7) dry this sample down just to dryness, do not overdry (which may form Nd-oxides which are difficult to get into solution again)

Because the capacities of the above columns are not sufficient for large samples, a different procedure must be used for sample sizes >100 mg. This procedure consists of only one column and is exactly the same one used for bulk separation of the REE for isotope dilution analysis (though columns for REE are kept separate from those used for Nd isotopic composition). This procedure is described in section II of this appendix, and was the one utilized in this study.

These first column passes are used in order to obtain a rough separation of most monovalent and divalent cations, and some trivalent cations from Nd, but do not separate Sm from Nd. The final column pass described below is used on all samples to effect this final separation.

The final column is made of pyrex glass and consists

of 0.2 I.D. x 35 cm capillary tubing with a 25 ml well attached for the effluent (Figure IA). The well has a ground glass joint and a cap with a compatible female joint. The cap in turn has a small section of hollow tubing protruding from the top to which a length of flexible Tygon tubing is attached. The Tygon tubing is attached to a double 2-gallon water jug apparatus which is used to achieve overpressures on the column, and thus decrease the elution time. (Because of the aspect ratio of the column used, a complete column run to elute Nd, without any overpressure, would take longer than a day.)

The separation takes between 3.5 to 6 hours depending upon the height of the upper 2-gallon jug or pressure applied to the column. There is, however, a "break-point" in the separation chemistry, where the rate of elution becomes too fast and equilibration of the resin with the eluent and REE is destroyed (Dan Unruh, personal communication). The elution time should be kept to a minimum of 4 hours.

The crucial step in this column pass is the loading procedure. The sample must be loaded in the smallest possible amount of HCl (<0.5 N). Greater amounts of liquid significantly decrease the efficiency of the separation.

Figure 1A:

Schematic diagram of the 0.2 x 35 cm elution column used for separation of Sm from Nd.

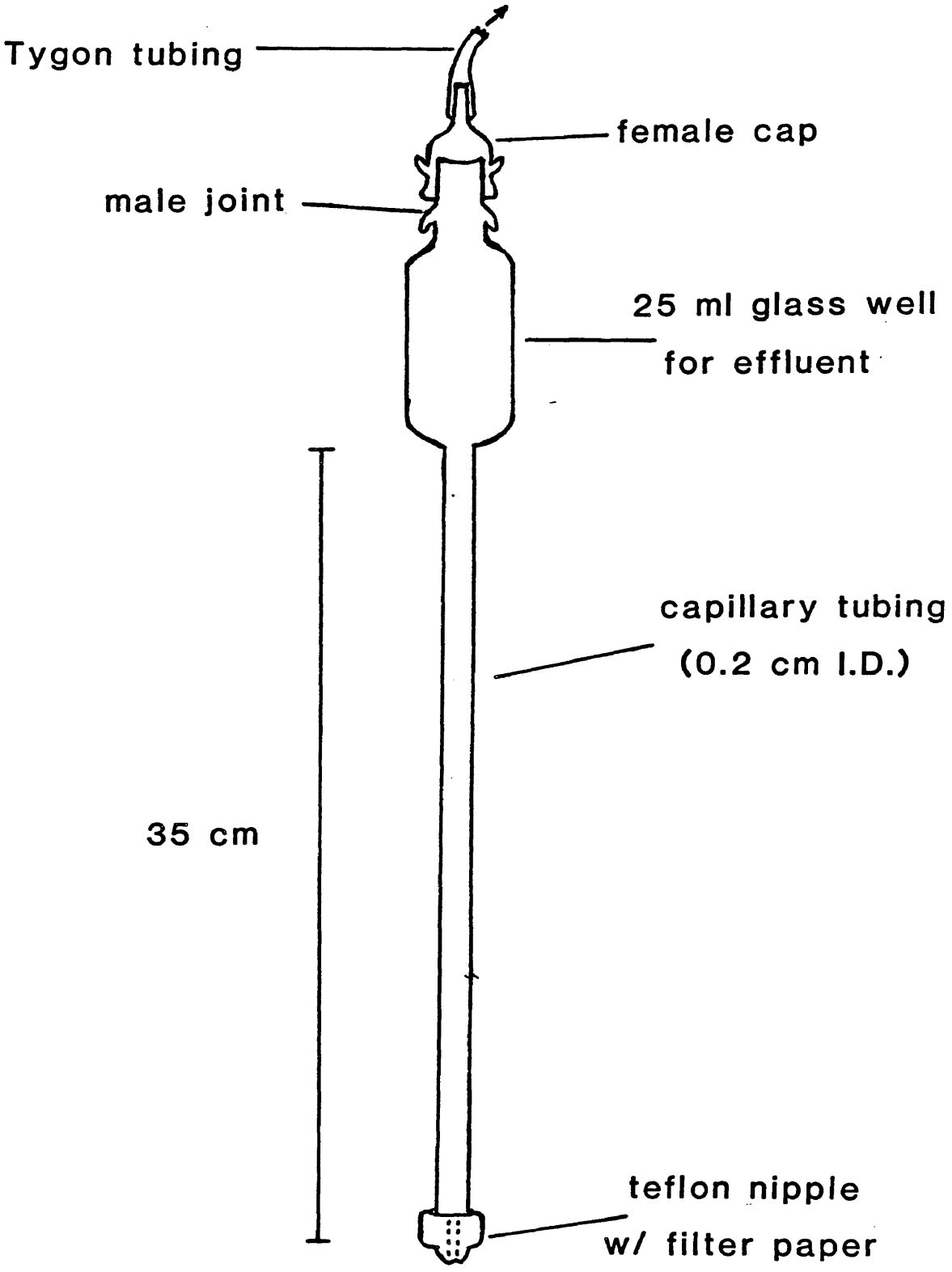
Tygon tubing
female cap
male joint
25 ml glass well
for effluent
capillary tubing
(0.2 cm I.D.)
35 cm
teflon nipple
w/ filter paper

Figure IA

(It is important to get the sample onto the thinnest layer of resin possible, in order that the elution not begin until the favored separation media, 2-methyllactic acid, is added.) It is also important during loading that the tip of the loading pipette touch only the resin or the inside of the capillary tubing, but never the glass well. Touching of the glass well will destroy the separation and even the yield. In touching the well a small amount of the sample may be left behind. Upon addition of the elluent, this will be brought into solution and eluted throughout the run time (DePaolo, 1978). We have found that making this mistake will increase the amount of Sm in the "Nd" fraction by up to a factor of 10.

The column is calibrated by adding known quantities of Sm and Nd onto the column and collecting 0.5 ml fractions throughout the elution. These fractions are then tested for the presence of the Sm and/or Nd and peak shapes are constructed. The full procedure is set forth in Shirey (1984) and below.

The indicator used to test for the presence of Sm and/or Nd is Eriochrome Black-T. This indicator will give a positive test for many cations including all of the REE, therefore all of the solutions used in calibrations should contain solely Sm and/or Nd. Both Sm and Nd can be run

through the column simultaneously for the calibration (there is a separation of over 1 ml between Sm and Nd on a well-maintained column), but the abundances must differ enough to be detectable in the titration. Reagents used in the titration are the following (Shirey, 1984):

EDTA (ethylenediaminetetraacetic acid):

-- concentrated stock solution (0.1 M):

29.21 g EDTA acid, 9.0 g NaOH; heat and stir together and dilute to 1 l with H_2O

-- dilute working solution (0.00001 M):

0.1 ml concentrated stock diluted to 1 l with H_2O

TEA (triethanolamine):

-- concentrated stock solution (1 M):

149.19 g TEA diluted to 1 l with H_2O

-- dilute working solution (0.1 M):

100 ml concentrated stock diluted to 1 l with H_2O

EBT (Eriochrome Black-T):

-- concentrated stock solution:

0.2 g EBT powder + 5 ml methanol + 15 ml 1 M TEA stock solution (shelf life $\leq$ 1 month)

-- dilute working solution:

2.2 ml EBT stock + 5 ml methanol + 15 ml 0.1

M dilute TEA

The calibration scheme is as follows (Shirey, 1984):

(1) collect 0.5 ml fractions in 30 ml teflon beakers

(2) add 1 ml of 1 N HCl to each fraction

(3) add 0.1 ml dilute EBT working solution to each fraction. All solutions will be pink in acid. EBT must be made up fresh (dilute solution lasts 2 days)

(4) add dilute working solution of TEA into teflon beakers until pH = 7.0 $\pm$ 0.2. At this point the EBT will be blue if no Sm or Nd is present, pink if some is present. If too much TEA is added, adjust pH down to 7 by adding HCl.

(5) maintaining a constant pH of 7.0 $\pm$ 0.2 (as the EDTA acid is added the pH may start to decrease; if this occurs then add a small amount of TEA to bring the pH back up to 7.0), titrate fraction with EDTA until solution color changes from pink to blue (endpoint is somewhat arbitrary, consistency is important here). Record amount of EDTA used (directly proportional to amount of Sm and/or Nd in the fraction, Figure IB).

Before the columns can be used for the Nd separation, a batch of column resin must be pre-treated and equilibrated with large volumes of 2-methyllactic acid

Figure 1B:

EDTA titration plot with known amounts of Nd. The plot is used as a calibration curve for determination of unknown amounts of Nd when calibrating the Nd column for peak shape information (the line is a visual fit of the points).

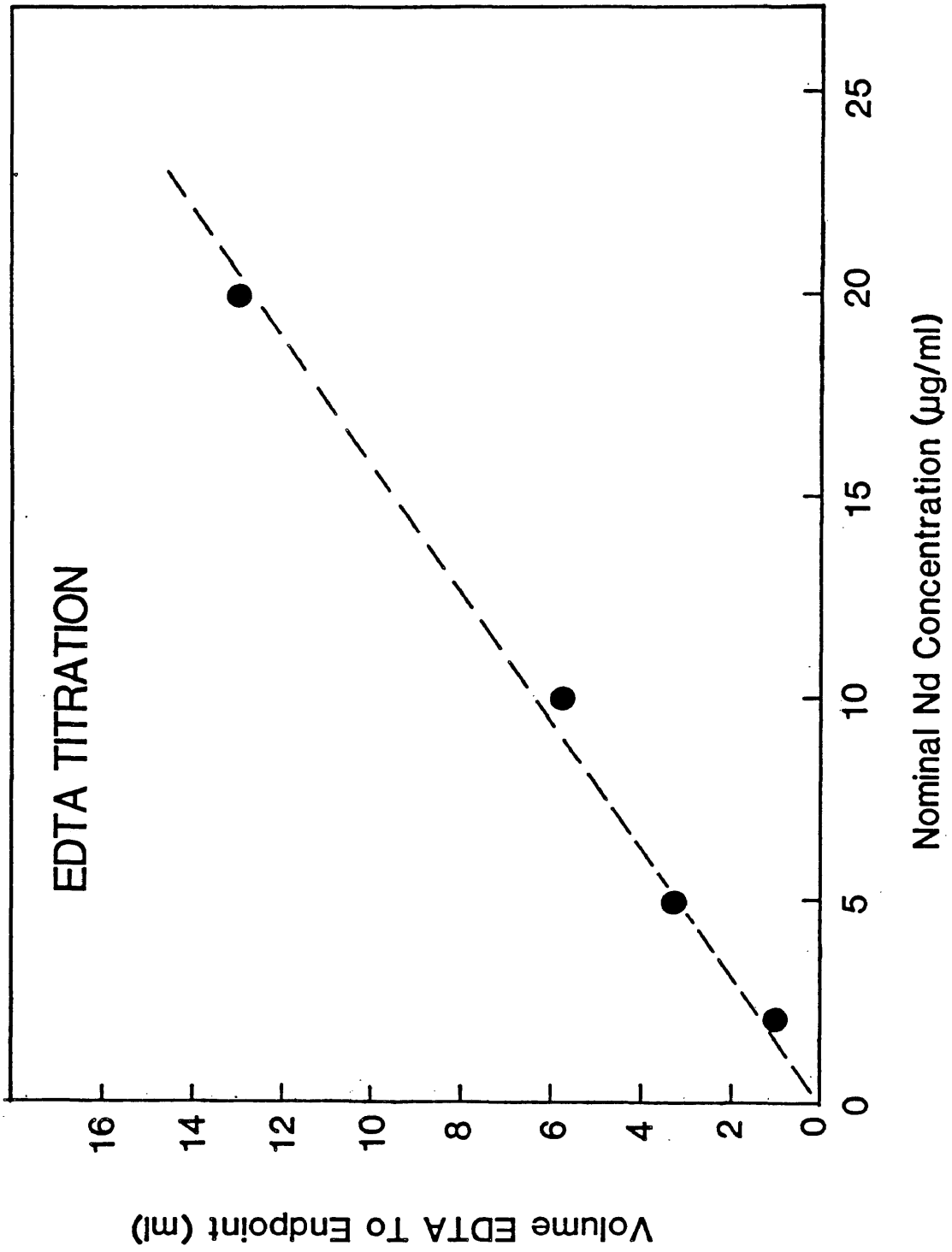
EDTA TITRATION
Volume EDTA To Endpoint (ml)
Nominal Nd Concentration (µg/ml)
0
2
4
6
8
10
12
14
16
0
5
10
15
20
25

Figure 18

using the method of Whitford, et al (1978). Approximately 100 ml of resin is placed in a pyrex column and rinsed thoroughly with several washings of 6N HCl. The resin is then treated with 1 liter of the elluent 2-methyllactic acid to remove all traces of HCl. Finally, the resin is stored in a teflon bottle in $3x H_2O$ until it is used for the separation.

The following procedure is used for the quantitative separation of Sm from Nd (modified and amplified from DePaolo, 1978, and Shirey, 1984):

(1) punch out a small piece of filter paper to fit into the teflon nipple.

(2) attach the nipple to the column, and add 15-20 ml of 3 x H_2O onto the column.

(3) affix cap over the well (the fit is made snug by a judicious use of silicon sealant and small rubber bands on matching arms of the well and the cap) and adjust the bottle apparatus to apply a pressure -- this is to remove bubbles in the capillary tubing.

(4) remove the cap to the column and lower bottle apparatus to remove overpressure.

(5) with some H_2O remaining in the well and tubing, pour on a slurry of AG50Wx4 (-400 mesh) resin (approximately 1 ml of resin).

(6) again apply an overpressure until all of the resin has compacted in the capillary tubing (this takes about 20-30 minutes).

(7) with a glass pipette remove excess resin from the well and the top 1 cm of the capillary tubing, and rinse the well thoroughly with $3\times H_2O$.

(8) add 8-10 ml of 0.2 M 2-methyllactic acid that has been adjusted to a pH of 4.50 $\pm$ 0.1 with ultrapure NH_4OH (this adjustment is best done with the use of a high quality pH-meter -- equipment from D. Langmuir'sresearch group was used in this study), and allow this to drip overnight, or if in a hurry, apply an overpressure for 2-3 hours (4-5 ml of effluent) -- to equilibrate the column.

(9) suck out excess 0.2 M 2-methyllactic acid with a pipette and load sample with a glass pipette in 0.1 ml dilute (<0.5 M) HCl onto top of resin bed without touching the glass well.

(10) wash with 0.3 ml $3\times H_2O$ (using a clean pipette).

(11) fill capillary tubing (using a clean pipette), up to the opening into the well, with 0.2 M 2-methyllactic acid and apply an overpressure.

(12) just before tubing runs dry remove the

overpressure and add 8-10 ml of 0.2 M 2-methyllactic acid, filling the capillary tubing first with a clean pipette, and then pouring the rest of the solution into the well.

(13) apply an overpressure and allow 5.5 ml of elluent to pass through --> discard.

(14) elute 2 ml of elluent --> collect in a 3 ml teflon beaker, Nd.

(15) dry sample in glass gas tank under heat lamp for 24 hours until dryness is just achieved (do not overdry) or (Shirey, 1984) treat sample with 1.5 ml 6 N HCl + 1 ml 6 N HNO_3 + 1 drop H_3PO_4 (or $HClO_4$) mixture and heat at 150°C until a very small honey-colored drop remains. H_3PO_4 is added to keep the sample from going to dryness. After a honey-colored drop is obtained, the sample can be taken just to dryness (again, do not overdry). Prepare sample for transportation to the USGS and loading into a mass-spectrometer as a phosphate on a Ta filament.

(16) the resin from the column is then drained into a teflon bottle containing 6N HCl.

(17) the column is rinsed thoroughly with warm 6N HCl followed finally by a 3xH_2O rinse to remove all Cl^-.

(18) the column is now ready for another elution for a new sample; start with (1) above.

The drained resin ("dirty" resin) from (16) is shaken daily and allowed to sit in HCl for approximately a week. At this time the HCl is discarded and a clean volume of HCl is added to the resin in the bottle. This procedure is repeated until the resin has been washed for 2-3 months. The resin is then clean and can be re-used.

APPENDIX II -- MASS SPECTROMETRY

After chemical separations were performed, samples were taken to dryness in clean 3-5 ml teflon beakers for transportation to the USGS--Isotope Branch for mass spectrometric analysis. The details of sample loading parameters are given in Table IIA.

The element Rb was analyzed on a 6" radius NBS Shields-type mass spectrometer. Isotope dilution analyses of the REE were all performed on a 12" radius NBS Shields-type mass spectrometer. Sr was analyzed for isotopic composition and concentration, and Nd was analyzed for isotopic composition on a VG Isotopes Micromass 54E 30cm (12") radius thermal ionization mass spectrometer.

All analyses performed on the Micromass 54E at the USGS were run in the automatic or semi-automatic mode using the computer program "DINGBAT" (Ludwig, 1982) or its successor "ANALYST" (Ludwig, 1985).

An additional goal of this study was to set-up a routine high-precision chemical procedure for separation of Nd from Sm at CSM. (Sm interferes with Nd isobarically at isotope 144, and because the nonradiogenic isotope ^{144}Nd is used to normalize all ratios measured on the mass spectrometer, one can see that this separation needs to be

Table IIA

Sample Loading Parameters for Mass-Spectrometry

Element	Isotope Comp.	Concent.	Filaments	Loaded as
Rb		X	Re-triple	chloride
Sr	X	X	Re-triple	chloride
Nd	X		Ta-sides, Re-center	phosphate
HREE		X	Re-triple	chloride
Gd(O)		X	Re-single	chloride/ nitrate
LREE		X	Re-triple	chloride

extremely quantitative.) This has included both the actual chemical separations and the analysis of pure standards and rock standards on the mass spectrometer.

Table IIB lists 13 separate analyses of the Cal-Tech Nd standard along with the accepted literature values. Plots of the values for isotopes 143, 145, and 150 normalized to ^{144}Nd for each run are given in figures IIA -C. The 13 runs for $^{143}Nd/^{144}Nd$ give an average value of 0.511897 $\pm$ 0.000014 (2-sigma). A standard such as this gives the analyst an idea of the precision of the instrument used for the analysis and the machine-bias between different labs. Relative to those measured at Cal-Tech, our $^{143}Nd/^{144}Nd$ ratios are low by a factor of 3.2×10^{-5} (due to inherent machine bias between labs). So, all values measured in our study can be brought into line with those at Cal-Tech by simply adding this factor to the measured $^{143}Nd/^{144}Nd$.

Due to the external error found in analyzing the Cal-Tech Nd standard, the within-run errors calculated for the $^{143}Nd/^{144}Nd$ ratios measured in this study cannot be lower than that found for the $^{143}Nd/^{144}Nd$ measured for the Cal-Tech Nd standard. This will increase some of the within-run errors, but it will give a much more realistic

Table IIB

Analyses of Cal-Tech Nd-isotope Standard

Run #	Date	$^{143}Nd/^{144}Nd$	$^{145}Nd/^{144}Nd$	$^{150}Nd/^{144}Nd$
1	4-20-85	.511920 ± 27		
2	4-21-85	.511965 ± 24		
3	5-04-85	.511812 ± 26	.348409 ± 18	.236561 ± 25
4	5-04-85	.511894 ± 10	.348406 ± 12	.236510 ± 28
5	5-10-85	.511886 ± 15	.348409 ± 7	.236468 ± 13
6	5-11-85	.511865 ± 16	.348393 ± 6	.236573 ± 34
7	5-11-85	.511921 ± 14	.348276 ± 8	.236462 ± 16
8	11-16-85	.511902 ± 14	.348422 ± 7	.236441 ± 14
9	11-17-85	.511903 ± 9	.348419 ± 5	.236458 ± 8
10	6-07-85	.511897 ± 15*		
11	6-08-85	.511902 ± 30*		
12	6-08-85	.511881 ± 41*		
13	6-28-85	.511899 ± 19*		
A@		.511897 ± 13	.348413 ± 11	.236489 ± 41
B		.511929 ± 8**		

*These samples were measured with the ^{150}Nd isotope spike, during its calibration.

@ Mean values and 2-sigma errors for all runs.

** Nominal value of the CIT-standard (Wasserburg, et al, 1981) recalculated using the normalization scheme of O'Nions, et al (1977).

Figure IIA:

Plot of within-run statistics for the $^{143}Nd/^{144}Nd$ ratios of 13 runs of the Cal-Tech standard with the average value (within the dashed lines). Bars on the points are 2-sigma errors.

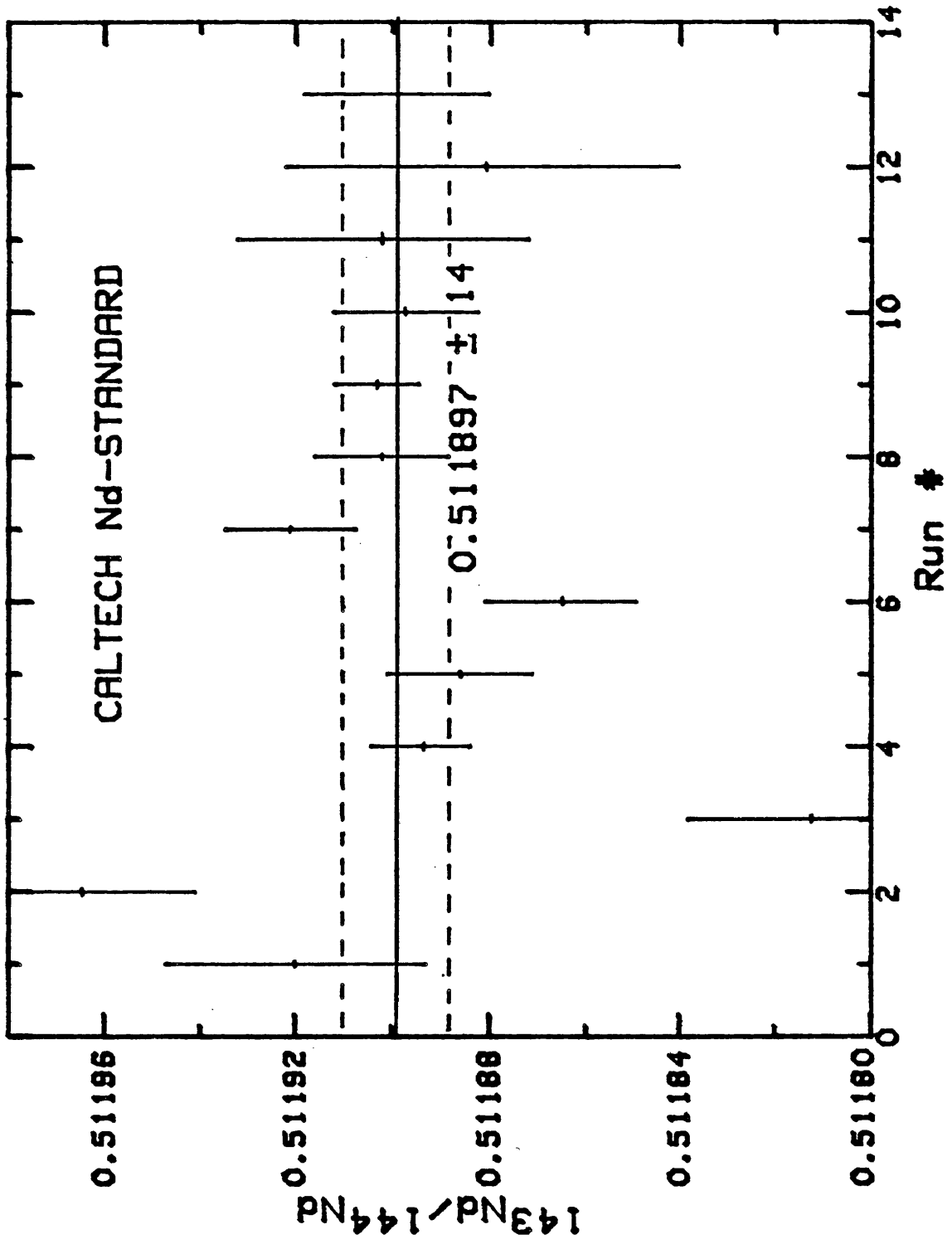
CALTECH Nd-STANDARD
0.511897 ± 14
$^{143}Nd/^{144}Nd$
0.51196
0.51192
0.51188
0.51184
0.51180
0
2
4
6
8
10
12
14
Run #

Figure IIA

Figure IIB:

Plot of within-run statistics for the $^{145}Nd/^{144}Nd$ ratios of 7 runs of the Cal-Tech standard with the average value (within the dashed lines). Bars on the points are 2-sigma errors.

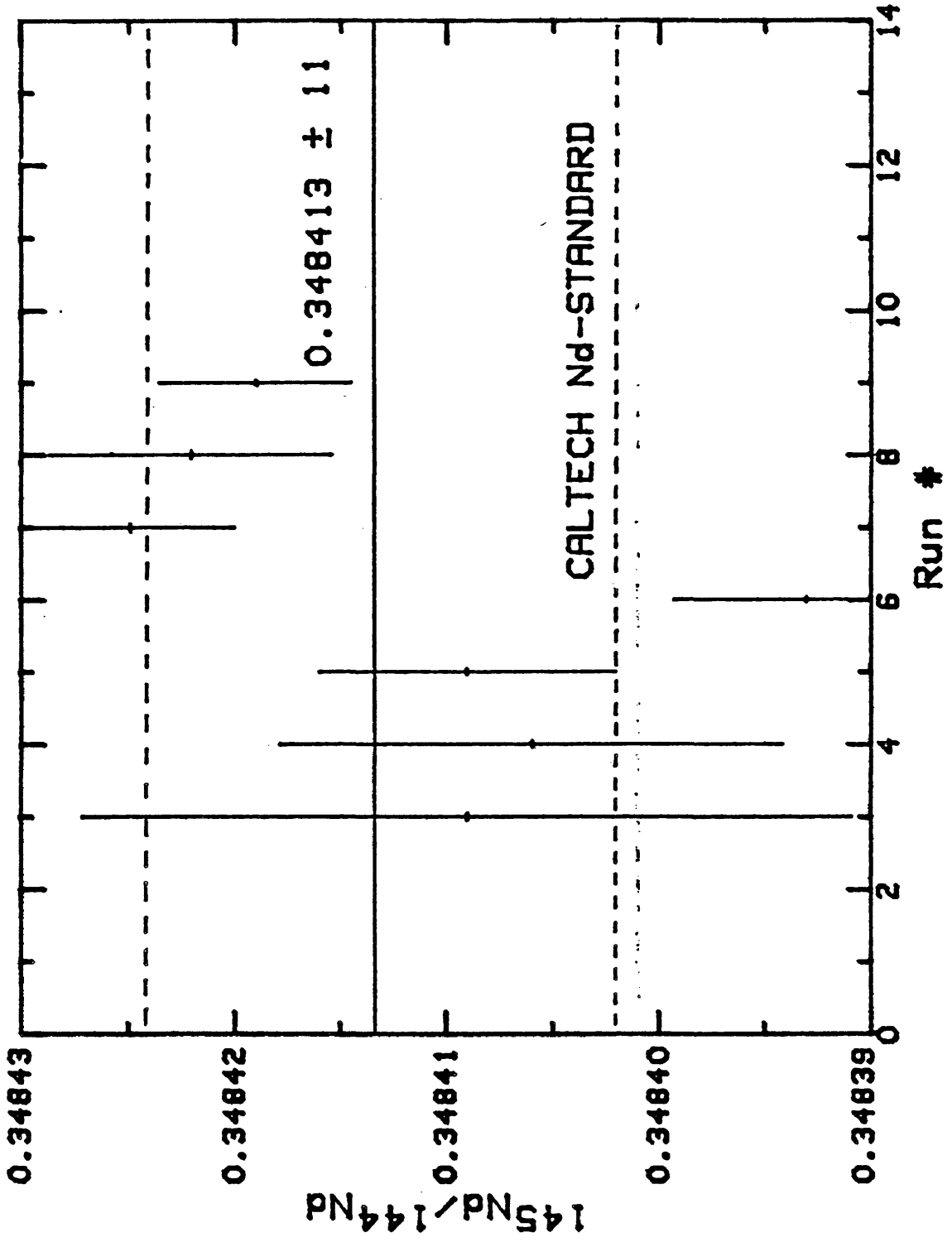
0.348413 ± 11
CALTECH Nd-STANDARD
Run #
0
2
4
6
8
10
12
14
0.34843
0.34842
0.34841
0.34840
0.34839
$^{145}Nd/^{144}Nd$

Figure IIB

Figure IIC:

Plot of within-run statistics for the $^{150}Nd/^{144}Nd$ ratios of 7 runs of the Cal-Tech standard with the average value (within the dashed lines). Bars on the points are 2-sigma errors.

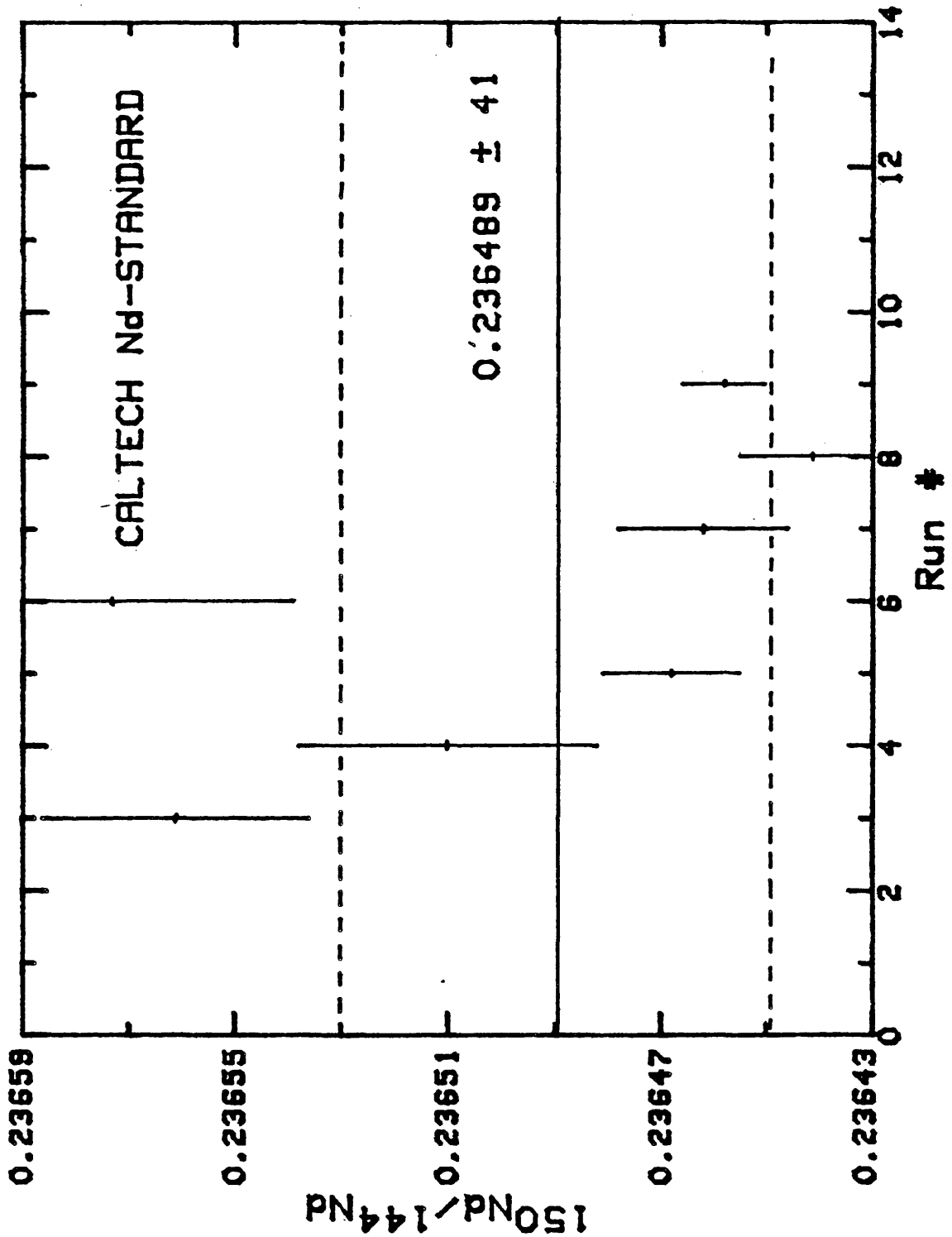
CALTECH Nd-STANDARD
0.236489 ± 41
$^{150}Nd/^{144}Nd$
0.23659
0.23655
0.23651
0.23647
0.23643
0
2
4
6
8
10
12
14
Run #

Figure IIC

estimate of the error in the analysis.

Rock standards were also measured in this study and are given in Table IIC along with published and accepted literature values for these samples. (M69/54 is an argillite sample from the Gunflint Iron Formation in Ontario donated by Peter Stille, and was chosen because of its relatively low abundance of Nd and extremely low $^{143}Nd/^{144}Nd$ compared to "normal" Nd. This sample is therefore an excellent indicator of any sort of contamination in the chemical procedures.) All analyses are within expected ranges and indicate the accuracy of the procedures used at CSM.

Three analyses of the Sr isotope standard SRM 987 are shown in Table IID along with published literature values.

The standard rock, BCR-1, was also analyzed by isotope dilution for the REE. Two successive analyses are shown in Table IIE along with literature values published in Hanson (1980) and Lambert (1982).

Table IIC
Nd Isotope Rock Standards

	$^{143}Nd/^{144}Nd$
BCR-1, #1	.512652 ± 52
BCR-1, #2	.512655 ± 14
BCR-1 *	.512620 ± 20
	.512650 ± 20
M69/54	.511264 ± 51
M69/54**	.511243 ± 23

* Literature values from O'Nions, et al (1977).
** Value from Stille and Clauer (1986).

Table IID
Sr Isotope Standard, SRM 987

	Date	$^{87}Sr/^{86}Sr$
Run #1	10-12-85	.710271 ± 96
Run #2	10-12-85	.710278 ± 42
Run #3	11-30-85	.710283 ± 27
Liter.	1985	.710275*

* Literature value used by Palmer and Elderfield (1985).

Table IIE

REE Standard, BCR-1

REE	Lambert[1]	Hanson[2]	Snyder(1)	Snyder(2)
Ce	53.8	53.9	53.5	-----
Nd	28.5	28.8	28.9	28.5
Sm	6.51	6.57	6.56	6.56
Eu	1.90	1.97	1.97	1.96
Gd	6.55	6.64	-----	-----
Dy	6.28	6.34	6.40	6.33
Er	3.60	3.60	3.40	3.46
Yb	3.36	3.42	3.40	3.28

---

[1] From Lambert (1982).

[2] From Hanson (1980).

APPENDIX III -- Extended Petrographic Descriptions and CIPW Norms

ERGS-1: is a fine-grained (< 0.1 mm grain size) clinopyroxene (cpx) -rich amphibolite. Polycrystalline amphibole is found within patches that also contain aggregations of garnet and magnetite. Fine-grained plagioclase is well-formed, bladed to acicular. Some small ragged cores of cpx remain within the hornblende but only appear optically under crossed nichols. Subhedral to euhedral garnet is often found along boundaries where hornblende and plagioclase are in contact.

ERGS-3: is a medium to fine-grained (0.1 to 0.4 mm) seriate-textured two- pyroxene gabbro. Pyroxenes (both orthopyroxene (opx) and cpx) are large (1 to 2 mm) and porphyritic in nature with interstitial finer-grained plagioclase. Pyroxenes often poikilitically enclose fine-grained subhedral grains of plagioclase. Plagioclase in the groundmass is typically subhedral to anhedral. Pyroxenes are enclosed by a thin rim of hornblende (green in plain light), especially where in contact with plagioclase. Small amounts of medium- to fine- grained garnet are in contact with opaques (magnetite), and both are often surrounded by a thin rim of of hornblende and adjacent to plagioclase - pyroxene contacts. Fine-grained

hornblende is also often found along contacts between plagioclase crystals. Opx (especially larger grains) appear to be zoned with darker brown rims in plain light. In one instance, a series of zoned pyroxenes surround a single interstitial anhedral magnetite (?) grain, the contacts containing a fine selvedge of hornblende. Finer-grained pyroxenes in variable states of alteration, some sieve-textured with patchy hornblende throughout. Biotite is a minor constituent found within hornblende patches. Extremely fine-grained magnetite can be enclosed by fine-grained garnet. Fine-grained magnetite can also be found within pyroxene. Plagioclase also appears to be zoned.

ERGS-4: is a medium-grained equigranular pyroxenite. Pyroxenes (0.2 to 0.6 mm for cpx and 0.2 to 2.0 mm for opx) are patchy with extensive exsolution lamellae (possibly opx-cpx exsolution within same grain). Some exsolution textures appear myrmekitic. Olivine (0.2 to 0.4 mm) is often rimmed by serpentine and then amphibole -- in some areas only a core of serpentine remains with olivine pseudomorphously replaced. Clots of alteration occur which consist of cores of serpentine surrounded by amphibole, garnet, and magnetite, respectively. Pyroxenes are found in variable states of alteration and can be

shredded along edges by alteration / recrystallization. Paired twins are common in cpx.

ERGS-5: is a fine-grained (0.1 to 0.5 mm) equigranular two-pyroxene gabbro. This sample is similar to ERGS-3, except large poikilitic pyroxenes are absent. Grain boundaries were originally straight and angular, but have become curved and lobate due to alteration by hornblende. Again, magnetite occurs along grain boundaries in association with hornblende. Pyroxenes appear to be in a more advanced state of alteration than in ERGS-3. Plagioclase is found in greater abundance than in ERGS-3. Some of the larger pyroxenes are again zoned, but zoning is not as obvious. Zoning of plagioclase is also evident. Acicular plagioclase is sub-ophitically surrounded by pyroxene in some cases. Plagioclase is somewhat more euhedral than in ERGS-3.

ERGS-6: is a fine-grained (0.2 to 0.4 mm) equigranular two-pyroxene gabbro. This sample is very similar to ERGS-5, except it contains very small amounts of fine- grained biotite. A small micro-fracture runs through this section and is easily distinguishable by the hornblende found in abundance as a linear array, altering all pyroxenes. Again, angular grain boundaries are found between minerals. Ragged anhedral hornblende rims

pyroxenes and occurs along grain boundaries between subhedral to euhedral elongate plagioclase crystals. Small amounts of chlorite occur along the micro-fracture. Very little if any garnet is found in this sample. Amorphous Fe-oxide (?) alteration can be seen along some grain boundaries. Substantial magnetite (?) can be seen which is anhedral and sieve-textured, and is enclosed by hornblende.

ERGS-7: is a medium- to coarse- grained cumulate -textured orthopyroxenite. The mineralogy consists almost totally of euhedral opx (0.1 to 1.5 mm) + anhedral and interstitial plagioclase (0.1 to 0.4 mm) with only a very small amount of subhedral to euhedral cpx (1.0 to 1.5 mm). Cpx is light brownish-green in plain light, while opx is colorless. Cpx also has higher order interference colors than opx. Cpx may have exsolved margins.

ERGS-9: is a medium- to coarse-grained, cumulate -textured olivine -rich picritic websterite. Poikilitic opx (0.2 to 1.0 mm) encloses small olivine (0.1 to 0.7 mm) phenocrysts. This sample is strictly an olivine - opx cumulate with some anhedral interstitial plagioclase (0.1 to 0.6 mm). Olivine has amphibolitized / serpentinized rims where in contact with plagioclase, except when enclosed by opx. Biotite and magnetite (?) are minor and are interstitial to the cumulates. Twinning occurs in

pyroxenes; one twin opx the other cpx.

ERGS-10: is a medium- to coarse- grained two-pyroxene gabbro. Anhedral grains of plagiocclase (0.2 to 0.4 mm) are found as inclusions in pyroxene. Elongated well-developed lathes of plagioclase (0.1 to 1.0 mm) are common. Areas occur where pyroxenes have been almost completely altered to hornblende, leaving shreds of pyroxene. Opxs (0.1 to 2.0 mm) tend to form larger phenocrysts than the augites (cpx, 0.1 to 0.5 mm), which are comparable in size to plagioclase.

ERGS-12: is a medium- to very coarse- grained cumulate- textured harzburgite. Large poikilitic opxs (7 to 10 mm) occur which often contain inclusions of forsteritic olivine (0.1 to 1.0 mm). Both pyroxene and olivine can have exsolved margins. Olivines within the pyroxenes have relatively unaltered margins, whereas olivines without the pyroxenes have altered rims of amphibole and/or serpentine. Augite (cpx, 0.1 to 1.0 mm) is minor. Some biotite occurs which is interstitial to cumulates along boundaries with plagioclase.

ERGS-13: is a medium- to coarse- grained cumulate-textured harzburgite. Pyroxenes can be poikilitic (2.0 to 5.0 mm) with inclusions of olivine (0.1 to 2.0 mm). One large (2 mm) euhedral olivine crystal contains a ragged

inclusion of opx. Olivine and pyroxene are quite fresh and are packed tightly with very little anhedral and interstitial plagioclase (0.1 to 0.5 mm). Where plagioclase is interstitial the olivines again have alteration rims of serpentine or amphibole.

ERGS-14: is a medium- to coarse- grained cumulate-textured orthopyroxenite. This sample contains mostly euhedral to subhedral opx (0.2 to 1.0 mm) with a small amount of cpx. Coarse- grained opx encloses fine- grained opx with some anhedral interstitial plagioclase (0.1 to 0.5 mm). A high birefringent material also occurs interstitial to pyroxene, and is clear in plain light (scapolite ?).

ERGS-15: is a medium- to coarse- grained cumulate-textured opx- rich picritic websterite. Olivines (0.2 to 0.5 mm) have thick coronas of some asbestiform serpentine with encircling corona of possibly amphibole, also asbestiform. Globular exsolution textures are seen in pyroxenes. Cpx (0.2 to 1 mm) appears to have a higher birefringence under crossed nichols than opx. Cpx appears greenish-brown in plain light and may show distinct twinning, whereas opx (0.2 to 1mm) is colorless to grey. Included olivines appear to have cracked surrounding pyroxenes during alteration or cooling. Ragged pieces of cpx occur in olivine. Small shreds of biotite can be found

in opx. Plagioclase appears to be late stage and interstitial. Towards one edge of the section alteration is more intense, invading pyroxenes internally. Magnetite (?) is patchy and is highly localized near alteration of olivine.

Notes

* Extensive petrographic studies on hundreds of ultramafic samples from the Laramie Range by G.L. Snyder at the USGS -- Denver have shown convincingly that chromite is an impotant phase in some samples. However, in our limited study we could not distinguish definitively between chromite and other opaques.

* Rock names for samples were determined by using the Streckeisen (1977) classification for the fine-grained dikes (samples ERGS-1, -3, -4, -5, and -6) and that of Irvine (1982) for cumulate- textured rocks (samples ERGS-7, -9, -10, -12, -13, -14, -15).

Table IIIA: CIPW Norms

Mafic Suite

Sample #	ERGS-1	ERGS-3	ERGS-5	ERGS-6	ERGS-10
Quartz	0.57	----	----	2.54	----
Corundum	----	----	----	----	----
Orthoclase	0.79	0.75	1.00	1.03	0.55
Albite	15.48	12.43	14.12	12.61	10.06
Anorthite	29.02	33.39	30.30	29.17	36.85
Nepheline	----	----	----	----	----
Diopside:					
Wollastonite	12.90	11.47	13.71	13.12	13.26
Enstatite	6.63	7.24	7.50	6.12	8.88
Ferrosilite	5.94	3.51	5.71	6.85	3.39
Hypersthene					
Enstatite	14.15	17.59	12.44	12.31	15.23
Ferrosilite	12.66	8.53	9.47	13.77	5.81
Olivine:					
Forsterite	----	2.66	2.29	----	3.78
Fayalite	----	1.42	1.92	----	1.59
Ilmenite	1.67	0.90	1.37	2.30	0.51
Apatite	0.19	0.11	0.15	0.18	0.08
Sum	100.00	100.00	100.00	100.00	100.00

Table IIIA (continued): CIPW Norms
(Calculated with total Fe as FeO)

Ultramafic Suite

Sample #	ERGS-4	ERGS-7	ERGS-9	ERGS-12	ERGS-13	ERGS-14	ERGS-15
Quartz	——	——	——	——	——	——	——
Corundum	——	——	——	——	——	——	——
Orthoclase	0.60	0.32	0.30	0.29	0.31	0.49	0.75
Albite	9.00	1.94	0.96	2.45	0.97	1.84	2.90
Anorthite	21.92	15.19	12.36	10.15	9.51	13.03	15.02
Nepheline	——	——	——	——	——	——	——
Diopside:							
Wollastonite	10.26	6.25	4.33	3.90	3.38	5.55	5.33
Enstatite	6.87	4.50	3.24	2.91	2.50	3.99	3.75
Ferrosilite	2.63	1.18	0.66	0.61	0.54	1.06	1.13
Hypersthene:							
Enstatite	22.24	48.09	12.92	9.82	30.85	53.58	38.79
Ferrosilite	8.50	12.58	2.63	2.05	6.68	14.19	11.68
Olivine:							
Forsterite	12.01	7.37	50.75	54.78	36.27	4.48	15.29
Fayalite	5.06	2.12	11.37	12.60	8.65	1.31	5.07
Ilmenite	0.79	0.42	0.43	0.39	0.32	0.48	0.51
Apatite	0.11	0.04	0.05	0.04	0.04	0.04	0.11
Sum	100.00	100.00	100.00	100.00	100.00	100.00	100.00